



# Application of nano-layers for the improvement of the cavitation resistance

## Master Thesis

*Study programme:*

N2301 Mechanical Engineering

*Study branch:*

Machines and Equipment Design

*Author:*

**Feben Tereffe Huluka**

*Thesis Supervisors:*

Ing. Miloš Müller, Ph.D.

Department of Power Engineering Equipment





## Master Thesis Assignment Form

# Application of nano-layers for the improvement of the cavitation resistance

*Name and surname:* **Feben Tereffe Huluka**  
*Identification number:* S18000190  
*Study programme:* N2301 Mechanical Engineering  
*Study branch:* Machines and Equipment Design  
*Assigning department:* Department of Power Engineering Equipment  
*Academic year:* **2019/2020**

### Rules for Elaboration:

- A research of the thin coating technologies for the improvement of the cavitation resistance of technical materials
- The description of key parameters influencing the cavitation resistance of the thin coating
- The assembly of an experimental setup for the testing of the cavitation resistance
- The preparation of samples with the different configurations of thin coatings
- The cavitation resistance testing of selected samples
- The evaluation of the results and classification of the most influencing parameters from experiment
- The recommendation of the best thin coating configuration and a recommendation for the applications

*Scope of Graphic Work:* 10  
*Scope of Report:* 50  
*Thesis Form:* printed/electronic  
*Thesis Language:* English



### List of Specialised Literature:

1. KIM, Ki-Han, Georges CHAHINE, Jean-Pierre FRANC a Ayat KARIMI. *Advanced experimental and numerical techniques for cavitation erosion prediction*. Dordrecht: Springer, [2014]. Fluid mechanics and its applications, v. 106.
2. FRANC, Jean-Pierre a Jean-Marie MICHEL. *Fundamentals of cavitation*. Boston: Kluwer Academic Publishers, c2004. ISBN 1402022328.
3. BRENNEN, Christopher E. *Cavitation and bubble dynamics*. New York: Cambridge University Press, c2014. ISBN 978-1-107-64476-2.
4. ALICJA, Krella a Andrzej CZYŻNIEWSKI. *Cavitation erosion resistance of Cr-N coating deposited on stainless steel*. *Wear*. 2006, 260(11), 1324-1332. DOI: 10.1016/j.wear.2005.09.018.

*Thesis Supervisors:* Ing. Miloš Müller, Ph.D.  
Department of Power Engineering Equipment

*Date of Thesis Assignment:* November 1, 2019

*Date of Thesis Submission:* April 30, 2021

prof. Dr. Ing. Petr Lenfeld  
Dean

L.S.

doc. Ing. Petra Dančová, Ph.D.  
Head of Department

## Declaration

I hereby certify, I, myself, have written my master thesis as an original and primary work using the literature listed below and consulting it with my thesis supervisor and my thesis counsellor.

I acknowledge that my bachelor master thesis is fully governed by Act No. 121/2000 Coll., the Copyright Act, in particular Article 60 – School Work.

I acknowledge that the Technical University of Liberec does not infringe my copyrights by using my master thesis for internal purposes of the Technical University of Liberec.

I am aware of my obligation to inform the Technical University of Liberec on having used or granted license to use the results of my master thesis; in such a case the Technical University of Liberec may require reimbursement of the costs incurred for creating the result up to their actual amount.

At the same time, I honestly declare that the text of the printed version of my master thesis is identical with the text of the electronic version uploaded into the IS/STAG.

I acknowledge that the Technical University of Liberec will make my master thesis public in accordance with paragraph 47b of Act No. 111/1998 Coll., on Higher Education Institutions and on Amendment to Other Acts (the Higher Education Act), as amended.

I am aware of the consequences which may under the Higher Education Act result from a breach of this declaration.

June 12, 2020

Feben Tereffe Huluka

## **Abstract**

Research on Nano layer coating application for the improvement of the resistance to cavitation erosion has been discussed. The coating was accomplished by Arc PVD method where the substrate was an aluminum alloy namely duralumin. A vibratory cavitation device at a constant amplitude was used to conduct the cavitation test on the coated and reference samples. The surface characterization during the incubation period was carried out with the help of a confocal microscope. The effect of roughness on the duration of the incubation period was analyzed and the failure mode was studied to examine the coating's behavior under cavitation. To better understand the response of the coatings to cavitation, further surface characterization was performed using SEM and Brinell hardness tester. This technique allows us to understand the failure mode of the coating and the influence of the different parameters that can affect the cavitation resistance. The influence of substrate hardness on the cavitation resistance was analyzed and discussed. The substrate's change in hardness is due to the coating process. For this reason, the influence of temperature and time during the application of the coating on the resistance to cavitation is discussed. All the data obtained from measurement were compared against a raw sample, which shows that the resistance of the coated samples all decreased. This is due to the change in the alloy's property during the coating process, which is explained in the chapter labeled discussion.

Key word – Cavitation , Coating, Incubation period, Arc PVD

## **Acknowledgment**

First and foremost I would like to thank God for giving me the strength to get through life.

I would like to express my gratitude to my supervisor, Ing. Milos Muller, Ph.D. for giving me the opportunity to do this research and providing guidance throughout. I am greatly indebted to Ing. Jan Hujer, Ph.D. who took his time off to help and assist me throughout the entire time. I am grateful for the advice and support provided for this work. I would also like to thank Ing. Anna Bakalova Ph.D. for assisting and advising me all the way. Additionally, I would like to thank Ing. Totka Bakalova, Ph.D, for supplying me with the samples and helping me analyze the data. Big thanks goes to Rhoda and Emmanuel, who have been my helping hand. I cannot put into words the gratitude I have for all the people that have helped me throughout this time. I hope to one day pay it back or forward. I am grateful to the Ministry of Education, Youth, and Sports for granting me the financial support in my master's study through the Czech Government Scholarship. And to my family, thank you for always supporting and believing in me.

This work was supported by the Student Grant Competition of the Technical University of Liberec under the project No. SGS-2020-5028.

## Contents

1. Literature Review .....	12
1.1 Cavitation .....	12
1.2 Type of Cavitation.....	13
1.3 Effect of Cavitation .....	14
1.4 Dynamics of the Cavitation Bubbles.....	14
1.5 Material response to Cavitation .....	16
1.6 Cavitation Erosion.....	17
1.7 Resistance to cavitation erosion .....	18
1.7.1 Cavitation resistance of Aluminum and its Alloys .....	19
1.7.2 Cavitation resistance of Coated Materials .....	20
2. Experimental Techniques .....	23
2.1 Coating Methods .....	23
2.2 Cavitation Testing .....	27
I. Vibratory cavitation erosion testing.....	28
II. Cavitating Liquid Jets .....	28
III. Cavitation tunnels .....	29
IV. Rotating disc apparatus.....	30
2.3 Measurement of Cavitation Erosion.....	30
3. Methodology.....	32
3.1 Sample Preparation Methods .....	32
3.1.1 Chemical Composition of Duralumin .....	32
3.1.2 Arc Physical Vapor Deposition .....	32
3.1.3 Grinding and Polishing .....	33
3.1.4 Cutting and Pressing .....	34
3.2 Vibration Apparatus .....	35
3.3 Surface Characterization and Analysis .....	36

4. Results .....	39
4.1 Cavitation Erosion.....	39
4.2 Erosion mechanism .....	41
4.3 Hardness .....	45
5. Discussion.....	46
6. Conclusion.....	49
Reference .....	50
Appendix I .....	57



### List of Symbols and Units

<b>Symbols</b>	<b>Description</b>	<b>Unit</b>
$R$	Bubble radius	[m]
$R(t)$	Bubble radius as a function of time	[m]
$\dot{R}$	First order derivative of bubble radius	[m/s]
$\ddot{R}$	Second order derivative of bubble radius	[m/s <sup>2</sup> ]
$R_0$	Initial bubble radius	[m]
$P(R)$	Boundary pressure	[Pa]
$P_v$	Vapor pressure of the liquid	[Pa]
$P_\infty$	liquid pressure at an infinite distance from the bubble	[Pa]
$p_i$	Pressure inside the bubble	[Pa]
$\rho$	Density of the liquid	[kg/m <sup>3</sup> ]
$R$	Distance from the center	[m]
$T$	Time	[s]
$u(r, t)$	Simultaneous velocity at a distance r from the center	[m/s]
$p(r, t)$	Pressure of the liquid at a known distance r and time	[Pa]
$P_{min}$	Minimum pressure of the flow field	[Pa]
$\sigma$	Surface tension coefficient	[N/m]
$\mu$	Liquid viscosity	[Pa s]
$p_c$	Critical pressure	[Pa]
$\Delta\varepsilon$	Mean strain	~
$\Delta t$	Peak duration	[sec]
$V$	Displacement velocity	[m/s]
$l$	Length	[m]

## List of Figures

Figure 1: Phase diagram.....	12
Figure 2: Schematic of a spherical bubble in an infinite liquid .....	15
Figure 3: Phase of cavitation erosion (12) .....	18
Figure 4: Schematic of cavitation erosion mechanism(42).....	21
Figure 5: Cavitation in a convergent-divergent tube (65).....	29
Figure 6: Test section in cavitation tunnel in Hohenwarte II pumped storage power plant in Germany (67).....	30
Figure 7: (A) Buehler 2 speed grinder-polisher, (B) MetaServ® 3000 variable speed grinder-polisher.....	34
Figure 8: (A) Struers' Secotom cutting machine (B) Struers CitoPress mounting press (C) Struers' Tegramin grinding and polishing (D) Hot pressed Samples .....	35
Figure 9: (A) Schematic diagram of Vibratory Cavitation Erosion Apparatus, (B).....	36
Figure 10: Definition of roughness parameter .....	37
Figure 11: SEM microscope test of samples with (a)CrN coating (b)TiCN coating (c) AlTiN coating (d) CrN/TiN coating (e) CrN/AlTiN coating .....	38
Figure 12: Cumulative mass loss under cavitation erosion test.....	39
Figure 13: Erosion rate in cavitation erosion test .....	40
Figure 14 : Cumulative mass loss in time of raw and reference sample.....	40
Figure 15: Effect of time and temperature of the coating process on the mass loss rate.....	41
Figure 16: TiCN coated sample (A) before cavitation test, (B) after 10:30 sec of exposure under cavitation and (C) after 40:30 sec exposure.....	42
Figure 17: Change in Sz with time .....	44
Figure 18: Effect of hardness on samples' cavitation resistance.....	45
Figure 19: Effect of temperature on hardness.....	47
Figure 20: relation between Vacuum pressure and mass loss slope .....	48

## List of Tables

Table 1: Chemical composition of Duralumin.....	32
Table 2: Parameters for ARC-PVD Coatings .....	33
Table 3: BHN Hardness of samples.....	37
Table 4: Surface morphology of the samples at different time period .....	43
Table 5: Mass loss data for raw sample .....	57
Table 6: Mass loss data for AlTiN coated sample .....	58
Table 7: Mass loss data for AlTiN/CrN coated sample .....	59
Table 8: Mass loss data for CrN Coated Sample .....	60
Table 9: Mass loss data for CrN/TiN coated sample .....	61
Table 10: Mass loss data for TiCN coated sample .....	62

## List of Abbreviation

CVD	Chemical Vapor Deposition
PVD	Physical Vapor Deposition
H	Hardness
E	Young's Modulus
Sz	Maximum Height (Roughness Parameter)
SEM	Scanning Electron Microscope
ASTM	American Society for Testing and Materials
BHN	Brinell Hardness Number

# 1. Literature Review

The chapter is an introduction to the general concept of cavitation and bubble dynamics. The effect of the cavitation specifically cavitation erosion is discussed. Material response to cavitation and what properties are resistant to the erosion has been reviewed. Special interest was taken on aluminum and its alloys.

## 1.1 Cavitation

Cavitation is a phenomenon that occurs in liquids as pressure changes lead to the nucleation and growth of bubbles which eventually collapse when the bubble is exposed to a solid surface or when the pressure has a lower pressure than the surrounding pressure. [1] The process is similar to boiling, as illustrated in Figure 1, in which the phase change (or the formation of bubbles) that occurs during boiling is due to an increase in temperature at constant pressure and the opposite holds for cavitation. The bubbles collapse leads to the formation of shockwaves and micro-jets as it implodes on a solid surface. The repeated collapse results in vibration and erosion damage to the material. This is commonly seen in hydraulic equipment such as pumps, valves, etc. [2]

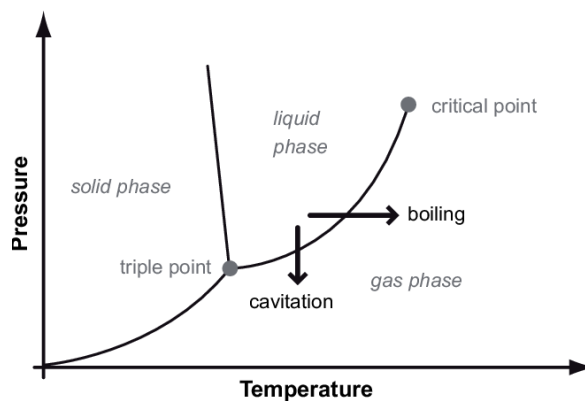


Figure 1: Phase diagram

The erosion arising from cavitation causes severe damage to materials, resulting in a decrease of efficiency and at times the material could fail if exposed to the shockwaves for a longer period. The cavitation phenomenon has been widely studied. This is to mitigate erosion damage. Several parameters affect the cavitation erosion which could be from the type of cavitation or the material's response to the surrounding liquid which depends on the mechanical properties of the material itself. These parameters are discussed in this chapter.

## 1.2 Type of Cavitation

There are two methods of classifying cavitation: (i) based on the cause of the cavitation and (ii) based on the physical forms of the bubbles.

### (i) Classification based on the cause of the cavitation

According to Lauterborn,[3], the classification of cavitation according to the causes of cavitation is either tension in the liquid or a local deposit of energy.

Cavitation due to tension can further be classified into hydrodynamic and acoustic [4]. Hydrodynamic cavitation is a phenomenon that occurs in flowing fluid with variation pressure arising from changes in velocity. Acoustic cavitation is a result of ultrasound waves passing through which results in pressure variation.

Cavitation due to local deposited energy is also further classified to optic and particle cavitation. The rupture of liquids due to high-intensity light or laser results in cavitation known as optic cavitation. And the rupture of any type of elementary particle (e.g., a proton) in liquids is called particle cavitation. [4]

### (ii) Classification based on the physical forms of the bubbles

From a physical point of view, three characteristic types (forms) of cavitation can be distinguished in water: vaporous, gas-vaporous, and gaseous cavitation.

Vaporous cavitation has wet saturated vapor in contact with the liquid within the cavitation zones. These types of cavitation are caused by a rapid increase in the internal partial vapor pressure, which blocks the diffusion of the gases dissolved into the bubble. The pressure that is generated upon cavitation collapse is extremely high and can cause severe damage. [2]

When bubbles are formed as a result of evaporation from the liquid and the diffusion of gases through the phase transition boundary layer, it is referred to as Gas-vapor cavitation. [5]. The phase transition is from liquid to wet saturated vapor-liquid. However, due to partial pressure difference, the gases released diffuses into expanding cavitation regions.

Gaseous cavitation is characterized by slowly growing and collapsing bubbles that are filled with gases released to the liquid. Consequently, it is not as violent or damaging as the other types of cavitation.

### 1.3 Effect of Cavitation

The cavitation bubbles created due to the decrease in pressure will implode after reaching a region of higher pressure. The implosion of the bubbles causes erosion, pressure fluctuation due to vibration, and noise which all of this create undesirable working condition and decreases the efficiency of the hydraulic system. It is also common to see these effects on automotive components such as cylinder, fuel jet pumps, injectors, valves, and the like.

The most common and widely discussed effect of cavitation is erosion. When the bubbles collapse near a surface, it causes shock pressure waves on the surface thus eroding it. This effect of cavitation is seen on valves, pipes, turbines, etc. It can also reduce the efficiency of a device if the vapor cavities are large enough to change the hydrodynamics of the flow through the system. At times this phenomenon can even lead to structural failure.

Even though the collapse of cavities is usually presented as a disadvantage, there are some fields where the effects were considered beneficial. Different chemical reactions favor the highly reactive radicals in the water system that is generated during the collapse of the bubbles. This is an effective method to divert impurities in wastewater. [6] It is also used to increase mixing and accelerate chemical reaction due to the turbulence created during cavitation. An example of this is the usage of cavitation in sonochemical synthesis. The specific chemical and physical effects of cavitation bubbles enable the synthesis of novel nanoparticle with various physicochemical properties [7].

### 1.4 Dynamics of the Cavitation Bubbles

The description of the dynamics of the cavitation bubble is best expressed by Rayleigh, who solved the problem of the collapse of an empty in a large mass of liquid. The boundary relation from the momentum equation obeyed the relation:

$$R\ddot{R} + \frac{3}{2}(\dot{R}^2) = \frac{p(R) - p_\infty}{\rho} \quad 1$$

Where  $p_\infty$  is the pressure of the liquid at an infinite distance from the bubble,  $\rho$  is the density of the liquid,  $p(R)$  is the boundary pressure. This relation is with the assumption that the effect of surface tension and liquid viscosity is neglected and the liquid considered incompressible. The assumption of incompressibility was because the liquid density and the dynamic viscosity is assumed to be constant. Furthermore, the content of the bubble is assumed to be homogenous and that the temperature and pressure within the bubble are always uniform. [8] The bubble is assumed to be spherical, with the radial position within the liquid will be denoted by the

distance,  $r$ , from the center of the bubble; the pressure,  $p(r, t)$ , radial outward velocity,  $u(r, t)$ , and temperature,  $T(r, t)$ , within the liquid will be so designated as seen in Figure 2. [8].

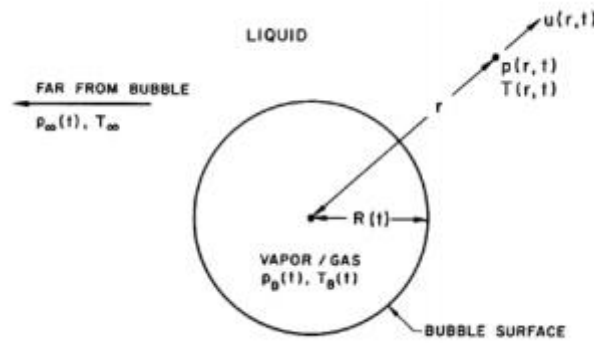


Figure 2: Schematic of a spherical bubble in an infinite liquid

This incompressibility of the liquid velocity is given by

$$u(r, t) = \frac{R^2}{r^2} \ddot{R} \quad 2$$

Using the Bernoulli equation, the pressure in the liquid is found to be

$$p(r, t) = p_\infty + \frac{R}{r} [p(R) - p_\infty] + \frac{1}{2} \rho \frac{R}{r} \ddot{R}^2 \left[1 - \left(\frac{R}{r}\right)^2\right] \quad 3$$

For Spherical bubble, viscosity affects only the boundary condition, resulting in the relation below

$$p(R) = p_i - \frac{2\delta}{R} - \frac{4\mu}{R} \ddot{R} \quad 4$$

Where  $p_i$  is the pressure inside the bubble,  $p(R)$  the boundary pressure of the liquid,  $\sigma$  the surface tension coefficient, and  $\mu$ , the liquid viscosity.

The description of the cavitation bubble growth and collapse in a liquid flow can be described using equation 1, but this by considering  $p_\infty$  as a function of time. The generalized Rayleigh equation in a view of equation 4 can then be written as[9]

$$R\ddot{R} + \frac{3}{2}(\dot{R})^2 = \frac{1}{\rho} \left\{ P_i - p_\infty - \frac{2\delta}{R} - \frac{4\mu}{R} \ddot{R} \right\} \quad 5$$

This relation is called Raleigh-Plesset equation, where  $P_i$  is the pressure in the gas at the bubble which is also a function of time. To describe the bubble dynamics for an inviscid flow, the equation is written as

$$R\ddot{R} + \frac{3}{2}\dot{R}^2 = \frac{1}{\rho}\{P_i - p_\infty - \frac{2\delta}{R}\} \quad 6$$

When considering bubbles, if surface tension, non-condensable gas, and viscosity are ignored, the bubble will remain in equilibrium before the initial time. The equilibrium bubble radius may be defined as

$$R_o = \frac{2\delta}{p_i - p_\infty} \quad 7$$

Where both  $p_i$  and  $p_\infty$  are functions of time. A bubble of this radius, before the initial time, will remain at rest if it is, to begin with at rest. But this equilibrium is unstable, at  $t=0$ , pressure being applied ( $p_\infty$ ) is higher than the pressure of vapor inside the bubble. This leads to the collapse of the bubble. The time when the bubble collapse is known as the Rayleigh time ( $\tau$ ). The time where the bubble completely collapses is expressed as:

$$\tau \cong 0.915 R_o \sqrt{\frac{\rho}{p_\infty - p_v}} \quad 8$$

Where  $p_v$  is the pressure inside the bubble. The evolution of the bubble at the end of the collapse is described by the following equation.

$$\frac{R}{R_o} \cong 1.87 \left[ \frac{\tau - t}{\tau} \right]^{\frac{2}{5}} \quad 9$$

Although the Rayleigh model is good for the analysis of bubble dynamics for short duration, it is not practical for real cases where successive collapse occurs where additional factors such as flow turbulence, pressure gradients, temperature, and gravity can affect the bubble's spherical shape. For these reasons, the Rayleigh model is only applicable to the study of spherical bubbles.

### 1.5 Material response to Cavitation

The bubbles formed during the change in pressure to below saturated vapor pressure exhibits high violent behavior. When the local pressure outside the bubbles rises, it results in explosive collapse. This process can also happen in the vicinity of a rigid body, which would result in a repeated impulsive load that has the potential to deform the surface of the solid wall. If the magnitude of the load is smaller than the critical mean stress the material will deform elastically. But the repeated actions of the bubbles or if the pressure pulses applied have a magnitude greater than the critical stress of the material it will lead to plastic deformation.



These deformations over some time increase the internal hardness of the material which is followed by the formation of pits leading to erosion and eventually failure.

A study conducted by Franc et al. [10] concluded that the damage occurring during cavitation cannot simply be correlated with the elastic limit but other parameters, such as strain rate plays a major role. The strain rate for many engineering materials can affect the failure and mechanical properties. The strain rate of cavitation impulsive loads can be estimated by two methods. The first is by the analysis of the imploding cavities or the second approach is from the strain dynamic concept of material deformations. [11] It is expressed as follows

$$\dot{\epsilon} = \frac{\Delta\epsilon}{\Delta t} = \frac{\Delta l}{l} * \frac{l}{\Delta t} = \frac{\Delta l}{\Delta t} * \frac{l}{l} = \frac{V}{l} \quad 10$$

Where  $\Delta\epsilon$  is the mean strain caused by an impulsive load,  $\Delta t$  is the peak duration,  $V$  is the displacement velocity of the impacted surface and  $l$  is the length of the plastic zone resulting from an impulsive load.

### **1.6 Cavitation Erosion**

The high impact pressure, which is generated by the implosion of bubbles, causes damage on the surface of solid material. This phenomenon is known as cavitation erosion (also called cavitation corrosion). [1] It can cause damage to fluid dynamic systems, such as pumps, ship propellers, and the like. The erosion leads to economic loss, a decrease in efficiency, and may lead to accidents as well.

The erosion caused by the imploding bubbles has phases it goes through before reaching the point of failure. These phases of the erosion of the material depend on the exposure time. The erosion rate to time graph (as seen in Figure 3) indicates four phases of the cavitation erosion process. The first period is the incubation period, where there is no measurable mass loss. During which the damage is limited where only small permanent plastic deformation or pits that have a very small diameter occur. This period usually doesn't last long, increasing the duration of this period would result in an improvement of the material's resistance to cavitation erosion. This can be done by surface treatment or providing a coating. As the exposure time increases the pits start to overlap, this leads to rapid depletion called the acceleration period. This is caused by the repeated impact of the cavitation bubble which induces micro-cracks and failures that eventually result in mass loss. The extent of this zone depends upon the strain-hardening properties of the material and involves microscopic chunks of material being removed following propagation of large cracks in between the grains of the material. [11] This

phase is observed in metallic materials. Brittle materials such as glass will fail before exhibiting measurable mass loss. After a certain amount of time, the erosion rate stops increasing and remains at a constant. This is the maximum erosion rate, where it will be followed by the decelerating stage. During the deceleration period, the surface topology has changed significantly that a new surface, with different roughness, affects the cavitation dynamics. This results in a lower mass loss, which is followed by the terminal stage (which is rarely exhibited). This is because in the practical application the material under cavitation would have already failed.

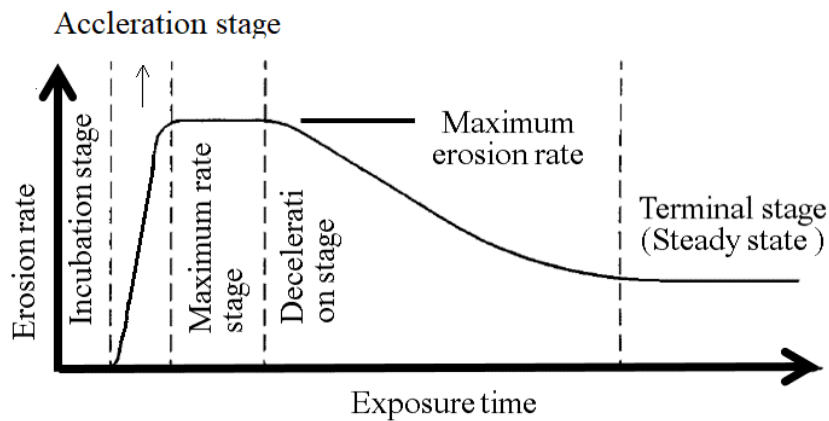


Figure 3: Phase of cavitation erosion [12]

The stages observed in the cavitation erosion do not only depend on the time of exposure but other factors such as the intensity of the phenomena, the fluid the material are immersed in and the mechanical properties of the material itself.

### 1.7 Resistance to cavitation erosion

Several studies [13–17] have been conducted to understand the cavitation erosion resistance of different materials, which stated that the most important property is the mechanical property namely the hardness, young modulus, fatigue strength, tensile strength. Other properties such as the grain size, chemical composition, and the surface roughness also affect the cavitation resistance of the material. Kreller [17] stated that if the material has discontinuity spots within the material it would contribute to the micro-crack initiation. This is because the discontinuity spot would be an area of stress pile up and nucleation.

The continuous collapse of bubbles on the material results in strain hardening, which causes damage similar to fatigue failure known as cavitation fatigue. This type of damage has been widely studied and the presumption of cavitation fatigue is based on the fatigue striations or

tire tracks like structures on the fracture surface [18–22]. For this reason, desirable mechanical properties of materials to resist cavitation erosion is considered to be high hardness and resistance to fatigue. Several studies[23–27] have found that hardness is a key parameter for cavitation erosion rate and its resistance as well. As hardness increases, the resistance to cavitation also increases but after reaching optimum hardness it would decrease. This is because the material’s stiffness would increase resulting in cracks while under cavitation. Liang et al [28] found that plasticity influences the erosion mechanism under cavitation. The higher energy is needed to fracture a material with higher plasticity than material with lower plasticity. For this reason, materials exhibiting lower plasticity it would undergo deformation and pits are formed faster and deeper.

Studies conducted by Krella et al. [29], found that parameter referred to as plasticity parameter (P), best represents the effect of elongation, impact energy, and hardness. It is represented as follows:

$$P = \frac{A * KV}{H} \quad 11$$

Where A is elongation, KV is impact energy and H is hardness. The increase of this parameter resulted in a decrease in the resistance to cavitation erosion. [29]

The grain size also has an effect on the resistance since the decrease in grain size results in better mechanical properties. In nanomaterials, the percentage of grain boundaries is higher than that in materials with higher grain size. And according to Hall-Petch rule, this results in a material with better hardness. [30]. Even though hardness increases with the increase of the percentage boundaries, it could also lead to deformation occurring from grain boundary sliding. This occurs if the grain sizes are too small (usually below 15nm) in turn causing a decrease in hardness [13].

### **1.7.1 Cavitation resistance of Aluminum and its Alloys**

Aluminum is a widely used metal due to abundant availability on earth. Even though it has some advantageous mechanical properties, it is one of the least erosion resistant material. [31] Aluminum alloys have a wide range of composition, which provides different properties and uses. Several studies[31–34] have been conducted to investigate the cavitation resistance of aluminum alloys. Vaidya and Preece [34] observed that as the alloying elements increases, the amount of deformation is smaller with pits in microscopic sizes. Plastic deformation and ductile

fracture were observed in dilute alloys. Thus the cavitation resistance of alloys can be adjusted by the amount of alloying elements.

A study conducted by Tomlinson and Matthews [31] showed that the alloys deformation mechanism is usually plastic deformation and ductile fracture. The investigation of Al-Si showed that it was the least resistant to cavitation erosion. It exhibited a high erosion rate coupled with the shortest incubation period. This was in comparison with Al-Zn which had a short incubation period but the erosion rate was low. This is due to the high strength and low erosion property of the alloy. Age hardening didn't have much effect for Al-Zn alloy but it was observed to have increased the incubation period of Al7Si alloy. They concluded that the best erosion resistant properties were found in mechanically alloyed materials. This could be attributed to the fact that the casting process generates defects such as porosities. This reduces the cavitation resistance of the alloys, regardless of the alloy composition. [35] In general aluminum's resistance to cavitation is affected by the type and number of an alloying element, and by microstructural properties such as grain size, microhardness, and like. [31, 34, 36]

### **1.7.2 Cavitation resistance of Coated Materials**

The application of coatings to reduce cavitation resistance has been studied extensively. Most studies noted that the properties of the coating material, the coating process, and the final properties of the coating can influence the resistance to cavitation erosion.

Several studies have noted that the nucleation center during the cavitation wear, is at the defects in the coating, but in general, coatings provide an improved cavitation erosion resistance. [13, 14, 37–40] There are more parameters to put into consideration to understand the resistance to wear of the coating one of which is adhesion. Different studies stated that the adhesion of coating material to the substrate as one of the main parameters that are essential in cavitation erosion resistance. [13, 14]. It has been proven that good adhesion increases the incubation period and protection from mass loss of the substrate material, whereas weak adhesion leads to the complete removal of the coating from the substrate. Weak adhesion can be caused by a thermal mismatch between the coating and the substrate or when the coating has local thermal softening, which indicates that temperature is another parameter affecting the coating and subsequently the resistance to cavitation erosion.

It is also necessary to consider the reaction of the coating material to the substrate. Ideally, a metallic coating applied to an alloy such as mild steel should form a continuous barrier that completely isolates the underlying metal from the environment. [41]. But this is not possible

because of discontinuities in the coating such as fine and gross pores arising from the method of coating and defects in the substrate resulting from fabrication and maltreatment in services, etc.[41]. These pores and pits act as a place of nucleation for the bubbles during cavitation. The bubbles that nucleate will grow and collapse further propagating the cracks and pits leading to delamination or failure in general. If the cracks on the surface of the material are perpendicular to the impact from the bubble, it leads to the deepening of the cracks, exposing the substrate. And if it is parallel the cracks extend to another adjacent crack or pores resulting in the peeling off of the coating.

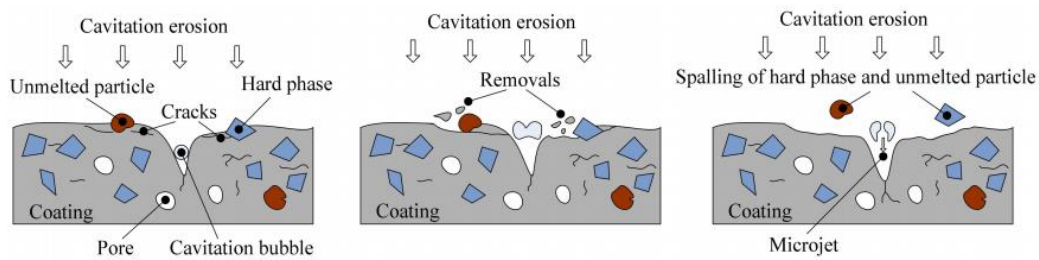


Figure 4: Schematic of cavitation erosion mechanism[42]

The other parameters that can increase the incubation period and reduce mass loss are the hardness and young's modulus. As the hardness of both the coating and the substrate increases so does the incubation period. However, if brittleness increases it will lead to failure. Chi et al. [43], stated that coating materials with higher ductility properties had better cavitation erosion resistance than those with high strength properties.

Krell et al. [44] specified that Young's modulus, which is the measure of the stiffness of a material, better represents coating behavior to cavitation degradation than hardness. The increase of young's modulus, which is also the increase of stiffness, means more energy is necessary to cause undulation of the coating. But after a certain point, further increasing the elastic modulus resulted in brittle fracture. That is characterized by deformations that accelerate the erosion rate.

Different authors [44, 45] have stated that to better analyze resistance to cavitation erosion of the coating and substrate, the plasticity index plays an important role. Plasticity index is expressed as follows

$$Plasticity\ Index = \frac{H}{E} \quad 12$$

Where H is hardness and E is young's modulus.

A study by Lima et al. [46] noted that the resistance of the WC-Co coating increases with decreasing the value of the plasticity index. An increase of the coating thickness has caused a decrease in the plasticity index, and with the decrease of the index, the impact-wear behavior of the system changes from brittle to ductile mode. [47].

Another important factor is the thickness of the coating material. According to A. Krella [47], increasing the coating thickness of TiN coating had a positive influence on the coating's mechanical properties. It increased the coating's stiffness and adhesion which results in an improvement in the resistance to cavitation erosion. But increasing the coating has its limits in the case of the application in fluid dynamic equipment. As the thickness increases the weight of the blade or propeller will also increase. That will result in the consumption of a larger amount of energy. In general, it was found that the wear mechanisms varied with thickness. However, no close relation has been set between the relation of coating thickness and wear resistance.

The chemical composition can also affect the resistance of the material to cavitation erosion. According to the studies conducted by Cui Lin et. al. [1], the increase of some elements, such as Mn, Co, Cr, C, and N, can improve the cavitation erosion. Coatings like AlTiN had proven to improve the resistance due to its superior hardness and elastic modulus.

Materials with smaller grain sizes but similar mechanical properties have better resistance to cavitation erosion than the larger grain size. An example is nanomaterials, which are characterized by high fatigue resistance and high hardness, have good resistance to cavitation resistance. [47]

## **2. Experimental Techniques**

This chapter discusses different methods of coating that can be applied to improve cavitation resistance. The methods of testing and evaluating materials resistance to cavitation are also presented below.

### **2.1 Coating Methods**

The need to increase the resistance of cavitation erosion through the coating is an ever-increasing search. The different coating methods that are commonly used differ from one another based on the deposition methods, which is also further differentiated based on different coating materials properties such as density, phase of the coating material, and more. As a result, mechanical stability, corrosion properties, biocompatibility (for biomedical applications), and enhancement of material behavior for a specific type of coating is affected by the selection of the method [48] Some of the common coating methods are spraying technology, electrochemical plating, and chemical and physical vapor deposition.

#### **Spraying Coating**

This coating method is a process of applying particles onto the surface through impact. Some of the commonly used technologies are discussed below

##### **I. Thermal Spray Coating**

Thermal spray coating is commonly used to increase the wear resistance of machines and equipment components. [49]. As the name indicates, it involves first melting the coating material, then spraying on the substrate. Once the sprayed particles reach the surface of the substrate, there is a thermal transfer from the particle to the substrate. The particles then solidify and contract which leads to mechanical bond and local fusion. This method can be applied for metal, ceramics, or polymers.

This method can be used to coat a large variety of materials at a high deposition rate compared to other coating processes. The possibility of being able to coat a wide range of coating thickness (from 15  $\mu\text{m}$  to a few mm) is another advantage of this process. [50, 51] . The disadvantage of this coating method is deposition efficiency, it could lead to overspray or under the spray. This results in a non-uniform coating or an undesired thickness in the coating.

## **II. Plasma Spraying**

Plasma spraying is a coating process in which molten or heat softened material onto the surface with help of plasma jet. The use of plasma jet means that there is a high energy heat source with a combination of high temperature, a relatively inert spraying medium, and high particle velocities. The coating material is injected into the high-temperature plasma flame which melts and is sprayed to the substrate to be coated. Several parameters can affect the adhesion of the coating material and substrate. The parameters could be grouped into properties of the components or properties of the coating process. The property of the components that heavily affect the adhesion to the substrate is the nature of the coating powder. Whereas the coating process parameters are energy input, torch geometry, distance from the substrate, and final coating/substrate cooling parameters.[52]

The advantage of this type of coating is that it can be used for different types of materials including materials with a very high melting point. The coating has high wear resistance, and high substrate adhesion as well. This coating method results in a lower porosity and homogeneous structure when compared to the thermal spraying process. But it is also a more complex process with a relatively high cost.

## **III. High-velocity oxygen fuel spraying (HVOF)**

High-velocity oxygen fuel spraying is a type of thermal spray coating where molten or semi-molten materials are sprayed at supersonic speeds. It is a high velocity, low-temperature spraying process which produces a dense metallic and hard facing coating [16]. This technique allows the application of metals, alloys, and ceramics as coating materials. At present, HVOF coating is often used to strengthen the surface of hydraulic mechanical materials. [42] This is due to the properties of the HVOF coating of low porosity and high adhesion.

In this technique, as with all thermal spray coating process, the coating material is first heated which is then fed into a combustion chamber. To obtain a gas stream for the coating, oxygen is added to the combustion chamber, where these ignite and react. The gas stream is then accelerated through a nozzle. The powder is added to the gas stream which melts and is deposited on the surface of the substrate [53]. The result of the thermal spray coating will be a thin overlapping platelet with high density. The drawback of this coating method is that its powder size required for the coating process is only acceptable in a small range with a narrow size distribution.



## **Electroplating**

Electroplating is a chemical or electrochemical process of coating for applying a metallic layer. To coat the substrate, it is wired as a cathode and the material to be deposited is wired as an anode. The cathode and anode are immersed in an electrolyte solution which is connected externally to a source of direct current. The positively charged cation of the metallic anode migrates to the cathode, where they are reduced to the metal and deposited as a thin layer.

The coating from this process has high hardness and good corrosion resistance. However, in this process, highly reactive materials can form an oxide layer when exposed to air, which has to be removed before electroplating. [16] The chemical surface treatment is used to prevent oxide formation during the plating process. [54]. For different material that is going to be coated different chemical treatment is necessary, which is another disadvantage of this process.

## **Vapor Deposition**

The coating of materials from a vapor state through a chemical reaction, condensation, or conversion is called vapor deposition. It can be categorized as either physical vapor deposition or chemical vapor deposition.

Vapor deposition is a process in which the coating material is a vapor state which is condensed through condensation, chemical reaction, or conversion to form a solid material. This process usually takes place inside a vacuum chamber. There are two categories of vapor deposition processes: Physical vapor deposition and chemical vapor deposition

### **I. Chemical Vapor Deposition**

Chemical vapor deposition (CVD) is one of the most used coating methods for a thin deposition. This method involves the deposition of the coating material, from a gaseous state, on to the substrate with dissociation and chemical reactions in an activated environment. The deposition is either homogeneous gas-phase reactions or heterogeneous chemical reactions that occur near a heated surface. In both cases, it leads to the formation of powders or films. [54].

There are different types of CVD process that is categorized into four main categories which are

- extraction & pyrometallurgy,
- electronic & optoelectronic materials,
- surface modification coatings, and
- ceramic fibers & Ceramic Matrix Composites.

CVD coating is capable to produce materials with a uniform coating on the substrate and high hardness value. The adhesion is also very good for a high deposition rate. Furthermore, it can be used for the production of multilayer and nanostructured coatings. But the chemicals used may be toxic, corrosive, and/or other safety hazards, which is dangerous during operation as well as during disposal of waste. The other drawback is that it needs an ultra-high vacuum and also requires heat resistant substrates.

## **II. Physical Vapor Deposition**

Physical vapor deposition (PVD) is an atomic coating method where the coating material (could be liquid or solid) is vaporized and deposited on the substrate. [15, 55–57]. This process is carried out in a vacuum and has four steps: (i) the coating material is evaporated to a vapor state (ii) the vapor is transported to the substrate, (iii) combination of the vapor with an active gas such as oxygen, or nitrogen and (iv) deposition of the vapor on the substrate which forms a thin film. [16]

PVD can be used for both single and multilayer coating, with a thickness in the range of a few nanometers to thousands. It is also used to prepare alloys compositions that cannot be produced by ingot metallurgy. [57] .It can be used for all types of inorganic and some organic materials. In comparison to other coatings, it is environmentally safer. However, the difficulty to coat complex shapes is a disadvantage. PVD is also a complex and expensive process due to the use of a vacuum or environment with very low pressure.

There are different methods of Physical Vapour Deposition coating. The commonly used methods are Evaporation, Sputtering, and Cathodic Arc. Evaporation PVD is the deposition of thin film by thermal vaporization. This type of coating is used for electrically conducting films, permeation barrier films on flexible packaging materials, etc. [56]. Sputter Deposition is a non-thermal deposition method of the thin film on the substrate through the impact of gaseous ions accelerated from a plasma where the surface atoms are physically dislodged from a solid surface. Sputter deposition is mainly used to deposit thin-film metallization on semiconductors and for the coating of magnetic films.

### **Cathodic Arc PVD Coating**

During Cathodic Arc Coating the substrate is electrically charged negative. The target becomes a cathode of an electrical arc. The substrate is then stricken with a high current, low voltage arc

which begins the evaporation process. The temperature starts to increase as the ions in the arc hit the cathode so the coating material is sprayed out at high velocity like a jet of vaporized material. The ion bombardment results in a coating with high adhesion. This type of coating method employs higher energy input as compared to the sputter PVD coating. The possibility of the presence or formation of macroparticles in the plasma stream is considered a disadvantage. This can be reduced by passing the plasma stream through a magnetic dust macro particle filter. [58]

Several parameters affect the quality of the coating. These could be grouped into either the substrates pretreatment or the coating process. The pretreatment which involves chemical, mechanical treatment, and drying plays an important role in the adhesion of the coating to the substrate. The coating process could be affected by several conditions such as coating time, coating temperature, plasma gases, or vacuum operation. But the most important parameters are cathode current, bias voltage, and reactive gas pressure. The temperature during the coating process plays a major role in the coating quality and substrate's properties. Temperature is not an independent variable, it is affected by the cathode current and bias voltage.

The thickness of a coating also affects the performance of a coated tool. Consistency in the coating thickness throughout the substrate can be attained by using different methods. The commonly employed method is using an array of permanent magnets in the form of a magnetic bucket. [59, 60] A study conducted by Keles et. al. [61] concluded that the thickness of a coating is impacted the most by cathode current. Then the bias voltage and gas pressure impact the thickness respectively.

A study conducted by Panjan et. al., [62] found that the heating time affects the defect density TiN coating. It was observed that during the heating process impurities to be generated can cause seed particles. That is particles lodged in-between the surface of the substrate and coating. This results in an increase in defect density which contributes to the loss in resistance of the cavitation erosion.

## **2.2 Cavitation Testing**

Cavitation erosion tests are done to evaluate different materials' resistance to cavitation erosion, which doesn't only depend on the properties of the material but also on the way the cavitation is generated. Different methods can be used in the laboratory and depending on how the cavitation is generated it is divided into four groups [11, 63]

- I. Vibratory apparatus (ASTM G-32)
- II. Cavitating liquid jets (ASTM G-134)
- III. Cavitation tunnels
- IV. Rotating disc apparatus.

But the two commonly used are the vibratory test method (ASTM G-32) and cavitating liquid jet method (ASTM G-134).

### **I. Vibratory cavitation erosion testing**

The vibration apparatus is the most commonly used testing method. It generates a cavity by utilizing an ultrasonic transducer which has a sonotrode (horn) attached to it. The transducer, driven by a power amplifier, generates vibration and transfers to the horn. And the vibratory motion of the horn generates pressure wave on to the surface of the test sample, which is immersed in water. These waves create cavities by continuous cyclic compression and tension forces. The amplitude and frequency of vibration are monitored, to give desired acoustic power output. During this time, the temperature has to be maintained at a specific temperature by submerging the beaker into a cooling bath, where the coolant (water) is constantly being circulated in the cooling bath.

The intensity of the pressure waves has an effect on the sample, where an increase in the intensity increases the cavitation erosion. This can be mitigated by creating a gap between the specimen and the horn. If the specimen attached to the specimen it is called the direct method. In the case where there is a gap between the specimen and the horn, referred to as the indirect method, the distance affects the cavitation load.

This testing device is a small scale and can perform the test in different liquids even with liquids with solid particles. However, the cavitation generated differs from hydraulic systems (flow devices in general). But it is still believed that the cavitation erosion that occurs on the sample is similar to flow devices.

### **II. Cavitating Liquid Jets**

Cavitating liquid jets was first established as a standard method under G134 by American Society for Testing and Materials (ASTM) in 1995. In this apparatus, cavitation is generated by utilizing a nozzle. The liquid which is at a high velocity is issued through the nozzle to generate the cavitation. To obtain the needed velocity for the test liquid, a pump is used. The cavitation bubbles collapse on the sample that is mounted coaxially with the nozzle. The test liquid is situated in a test chamber at a specified constant temperature and pressure.

The bubbles occur in the nozzle when the environmental pressure is smaller than the saturated vapor pressure. From Figure 5,  $P_c$  is the absolute pressure at the converging part of the nozzle. Cavitation occurs as  $P_c$  is smaller than the absolute saturated vapor pressure of the liquid without any change in temperature.

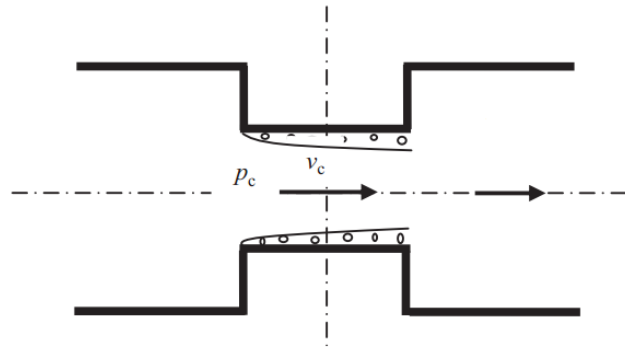


*Figure 5: Cavitation in a convergent-divergent tube [64]*

The cavitation produced by this type of apparatus has more realistic bubble clouds as compared to the vibratory cavitation apparatus. The intensity can also be adjusted by controlling the parameters. The parameters are the type of the jet, the jet's diameter, angle, and velocity, and the standoff distance. This gives the apparatus flexibility that is favorable for testing the different material's behavior under cavitation.

### **III. Cavitation tunnels**

Cavitation tunnels are larger much in size and produce a more realistic cavitation erosion. But it is not an ASTM standardized testing equipment yet. [12] This testing is carried out in a tunnel that has either cavitation such as wedges or the tunnel has a venturi effect to generate the cavitation. The tunnel that has hydrofoil which is inserted into the test section. The other advantage of the cavitation tunnel is that it is possible to observe the various zones of the cavitation phenomenon. This is possible because the test chamber has a viewfinder and the sample is placed in the wall of the canal. [65].

The flow velocity affects the cavitation intensity, where can result in a higher erosion arising from a more aggressive cavitation phenomenon. It is controlled by valves that are found at the inlet and outlet of the test chamber. The valves control the pressure inside the chamber which influences the flow velocity. The shape of the cavitator also can influence the intensity of the cavitation (cavitation erosion).

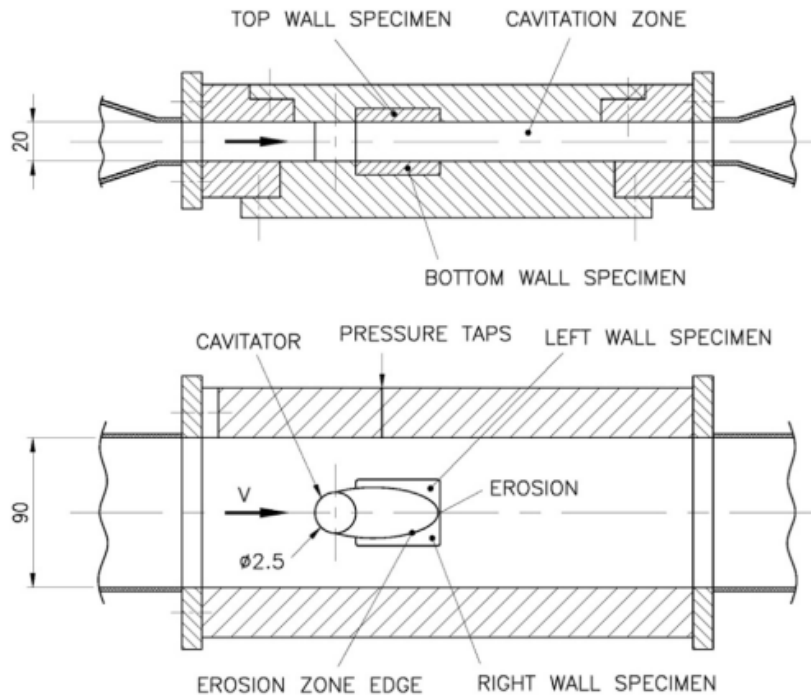


Figure 6: Test section in cavitation tunnel in Hohenwarte II pumped storage power plant in Germany [66]

#### IV. Rotating disc apparatus.

This apparatus generates cavitation by putting in use a disk that has cylindrical bolts or several holes with various radii. The disk rotates in a stationary test liquid which creates the cavitation in the holes or pins, the bubble then collapses on the test samples that are situated on the disc surface. The advantage of this testing apparatus is the ability to test several samples at the same time. Since it also resembles pump impellers, it would result in a more accurate experimental setup for hydraulic turbomachines. The major disadvantage is that it requires a longer amount of time to achieve the steady-state cavitation intensity. [66]

#### 2.3 Measurement of Cavitation Erosion

There are different methods of measuring the cavitation erosion of the material under the impact. Some of the most commonly used are mass loss, volume loss pit depth, and pit number. Mass and volume loss, which are relatively easier, measure the difference of both mass and volume respectively, before and after cavitation erosion. But these methods are not applicable when the plasticity of the material is large and, after cavitation erosion, the material is plastically deformed only but has no mass loss or with a small volume loss[1].

The Mass loss can be used to find the incubation period of the samples, as there would be no mass loss at this period. The cumulative erosion rate is the change in the mass loss in some duration per unit time. It helps find the rate at which the material is eroding after the end of the incubation period.

The negligible mass loss during the incubation period is studied by observing the pit depth and number. For better observation of the pits, the test samples must have a polished surface. The pit depth observed on the surface during the experiment varies. For this reason, the average depth is commonly used. And the measurement of the pit number, which can help characterize the aggressiveness of the flow.[11]

The selection of the appropriate time to perform the pit test needs careful consideration because as the exposure time increases the pits formed on the surface increase and overlap. It could result in the phase transition of the sample from incubation to accelerated mass loss. It could also result in the sample's failure. The threshold usually considered for the selection of appropriate time is yield stress.

During the analysis of the size of the pits on the surface of the sample, only the pits that contributed the largest to the erosion are considered. This is because the small pits, due to their small area are negligible. Also when considering an exponential distribution, the largest pits to the covered surface has a small number density, thus are neglected. [11]. Pitting on samples can be tested using contact profilometer, optical profilometer, laser interferometry, or scanning electron microscopy.

### 3. Methodology

This chapter describes the procedures taken for the experiment. The preparation of the samples and the experimental design are discussed below.

#### 3.1 Sample Preparation Methods

Aluminum alloys have widely been used for the production of parts that can cause it to undergo cavitation erosion such as ad valves, hydrofoils, etc [67]. Duralumin, which is an alloy of aluminum, copper, and magnesium, is typically used for casing components like water and fuel pumps, valves, propellers, etc. Duralumin has been recorded as having good mechanical properties but low resistance to corrosion. The individual admixtures of the components of the Duralumin influence the final property of the alloy. The experiment was conducted on single-layered and multilayered coatings which have duralumin as a substrate. There are two reference samples used in this experiment. The first reference referred to as the ‘raw material’, is a duralumin sample with the same chemical composition as the substrates of the coated samples. The second reference sample also has the same chemical composition as well but the sample was first coated with CrN which is then removed. This is to analyze the coating process effect on the substrate itself.

##### 3.1.1 Chemical Composition of Duralumin

The chemical composition of the duralumin used as a substrate according to SEM analysis was found to be as follows.

*Table 1: Chemical composition of Duralumin*

Elements	Wt. %
Mg	1.3 ± 0.1
Al	95.2 ± 0.2
Cu	3.5 ± 0.2

##### 3.1.2 Arc Physical Vapor Deposition

The experiment was conducted on seven samples, three of which are single layer coatings, two were multilayers and the last two were reference samples. The single-layered were coated with AlTiN, CrN, and TiCN while the multilayered samples were CrN/AlTiN and CrN/TiN.



The coated samples were prepared on a disk of  $\text{Ø } 25 \text{ mm} \times 5 \text{ mm}$  substrate at different temperatures with cathodes that best suit the type of coating. The parameters for each type of coating are listed in *Table 2*.

*Table 2: Parameters for ARC-PVD Coatings*

Parameters	Coatings				
	CrN/TiN	TiCN	AlTiN	CrN/AlTiN	CrN
Arc Current	70 A	85 A	70 A	60A	70 A
Coating temperature	300 °C	400 °C	280 °C	280 °C	280 °C
Negative bias voltage	80 V	40 V	85 V	75 V	75 V
Time of deposition	60 min	120 min	60 Min	30 min	120 min
Pressure of nitrogen in vacuum chamber	0.35 Pa	0.5 Pa	0.2 Pa	0.3 Pa	0.3 Pa

To increase the adhesion of CrN, AlTiN, CrN/AlTiN, and CrN/TiN coating to the substrate, the substrate was first cleaned with an alkaline solution in an ultrasonic bath for 5min, then rinsed in de-ionized water and dried with boiling ethanol and hot air. The substrate is then mounted on to the holder which is in a vacuum chamber where it is cleaned with Cr-ions to remove any traces of surface contamination and the native oxide layer at a bias voltage of 1000 V and Ar pressure of 0.2 Pa.[68, 69]. Before the coating was applied, contact interlayers of Cr and a 100nm thickness of CrN which is a transition film were deposited to improve the adhesion strength.

For TiCN coating, the discs were cleaned in acetone and ethanol for 5minutes, followed immediately by placing the substrate into a vacuum chamber. The substrate was then bombarded titanium ions after being cleaned in glow discharge of argon plasma. Layers of Ti and TiN are deposited on to the surface that acts as a contact transition. This is to increase the adhesion of the coating with the substrate. [68, 69]

### 3.1.3 Grinding and Polishing

The surface morphology of the sample affects the cavitation erosion process, as regions with higher roughness could be a source of nucleation for cavitation. To investigate the resistance to cavitation of the reference sample it is necessary to grind and polish. This helps to obtain a surface with a lower roughness. The reference sample was first placed on to Buehler 2 speed grinder. The grinding paper first used is silicon carbide with 220 Grit. The grinding paper is placed onto a rotating disc where the surface of the sample would be in contact. Tap water is

run on the grinding paper to reduce the increase of temperature due to friction between the surface of the paper and the sample. After a certain amount of time, the paper is changed to a finer grit paper of 300 Grit. The same process is repeated and the sample is then rinsed off with water and cleaning alcohol. Following the grinding process, the sample is polished which results in a mirror-like surface finish. This was accomplished by using a variable grinder polisher, which is composed of a plate that rotates at an adjustable speed. Particle suspension of  $9\mu\text{m}$  size is applied to the surface of the plate. Since the size of the particles is small, it is necessary to clean the sample not to transfer small particles which could disrupt the polishing process. The sample is cleaned using distilled water and polished. This process is repeated using an even finer suspension of nano-crystalline diamond suspension with a  $3\mu\text{m}$  size and a non-crystallized colloidal silica polishing suspension.

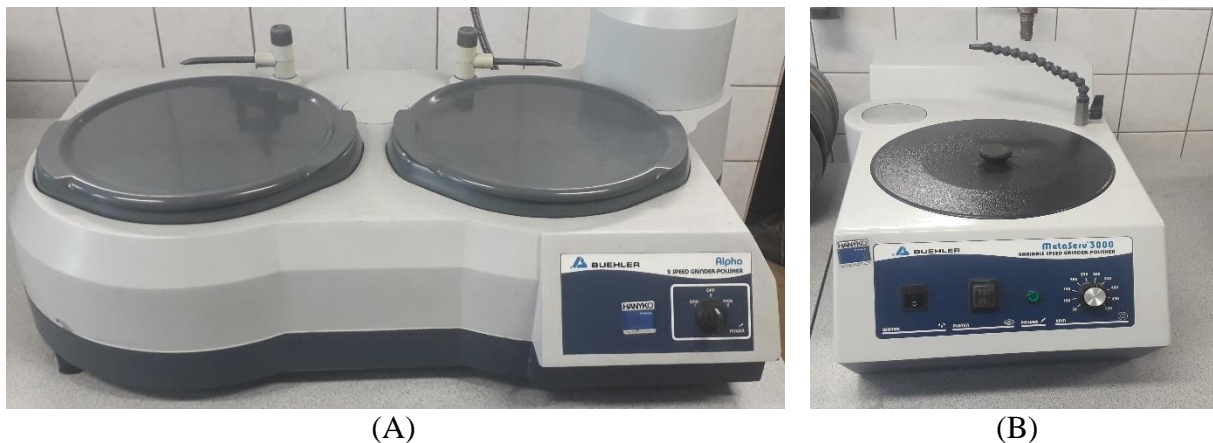


Figure 7: (A) Buehler 2 speed grinder-polisher, (B) MetaServ® 3000 variable speed grinder-polisher

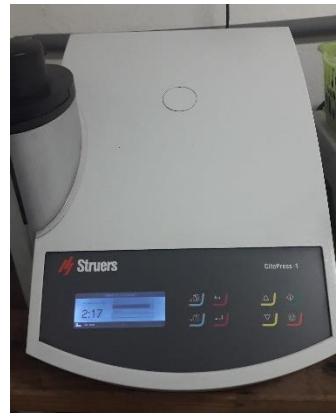
### 3.1.4 Cutting and Pressing

The surface characterization was using a Scanning Electron Microscope and Brinell hardness tester. To accomplish this, the samples were mounted in resin and polished. The first step in the preparation was to cut the samples into the desired size by using a high precision Struers' Secotom cut-off machine. Water is poured onto the cutting blade to reduce overheating during the cutting process. The sample is then hot mounted using resin for precision to investigate the area of interest. The resin used is Multifast red, which is a thermosetting resin that is cured at an elevated temperature. The sample is cleaned, dried, and placed on to the mounting cylinder where the resin is added. Water cooling is used to obtain the shortest possible mounting time. The samples are then polished using Struers' Tegramin grinding and polishing system. The samples were mounted to the holder then the grinding process was carried out with 4 different SiC foils with grits of 500, 1200, 2000, and 4000. Water is used as a lubricant. The samples

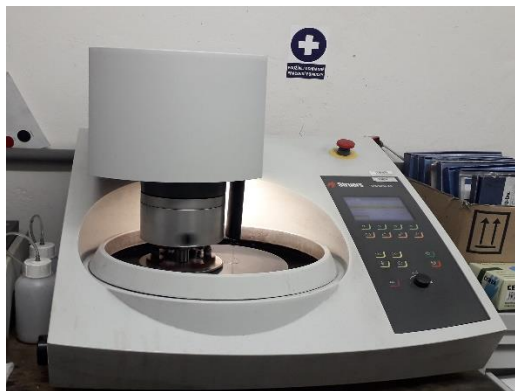
are then polished using aluminum and silica oxide as the suspension on the polishing cloth. This results in a mirror-like finish. But since the resin is not conductive, a thin conductive layer was applied on to the surface making the resin mounted sample conductive for SEM analysis.



(A)



(B)



(C)

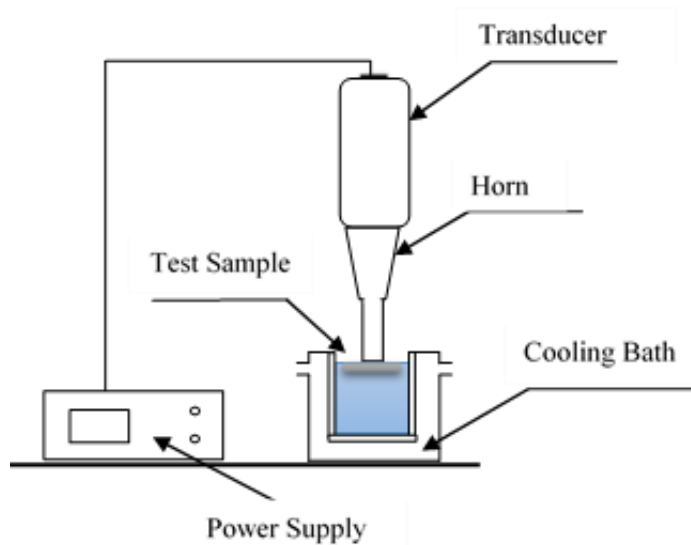


(D)

*Figure 8: (A) Struers' Secotom cutting machine (B) Struers CitoPress mounting press (C) Struers' Tegramin grinding and polishing (D) Hot pressed Samples*

### **3.2 Vibration Apparatus**

The cavitation tests were carried out by using a modified ASTM G32 vibratory apparatus with a stationary specimen. It consisted of an ultrasonic device that can produce frequency up to 20Hz and the vibration amplitude of 50 $\mu$ m. A 5mm gap was left between the specimen and the horn tip. The temperature of the test liquid was maintained at 23 $\pm$ 1 $^{\circ}$ C by constantly circulating in the coolant (water). The schematic diagram is as shown in the figure below.



(A)



(B)

Figure 9: (A) Schematic diagram of Vibratory Cavitation Erosion Apparatus, (B)

During the cavitation test, the sample was positioned in the center of the holder and fastened to the ultrasonic transducer by nuts and washer. The sample is immersed in the test liquid, which is distilled water for these tests.

### 3.3 Surface Characterization and Analysis

The surface characterization and analysis of the samples was accomplished through the data collected from mass balance, confocal microscope, scanning microscope, and Brinell hardness tester. The difference in the mass through time was used to obtain the duration of the incubation period and the mass-loss rate. These data can be used to analyze the resistance of the coating to the cavitation test.

To investigate the properties of the coating during the incubation period, the test was interrupted after a short duration and weighted using a mass balance. The worn surface was also analyzed to measure the surface roughness, using the Sensofar confocal microscope. The surface roughness has been proven to affect the erosion rate. The existence of cracks, un-melted particles, or pores can propagate under the cavitation test. Thus measuring the initial roughness of the samples helps understand the mass-loss rate. Furthermore, the propagation of the roughness throughout the cavitation test can be useful to analyze the deformation process of the coating. The roughness ( $S_z$ ) was found according to ISO-25178 standard.  $S_z$  is defined as the sum of the largest peak height value and the largest pit depth value within the defined area. In Figure 10,  $R_z$  (maximum profile height) is presented.  $S_z$  is the areal extension of  $R_z$ .

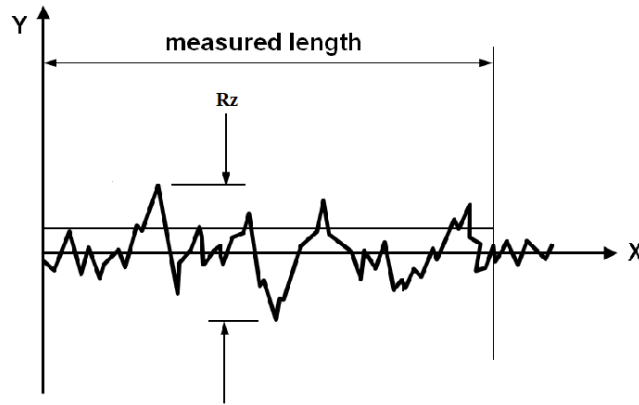


Figure 10: Definition of roughness parameter

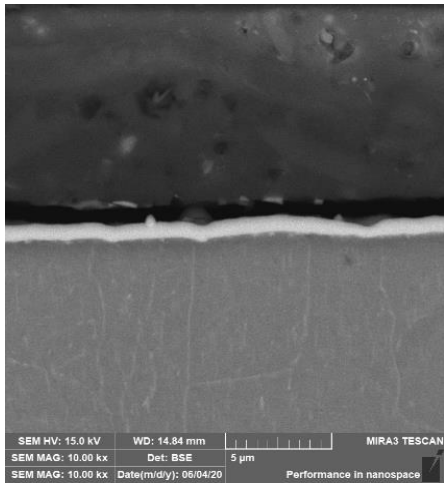
The analysis of the images obtained from a confocal microscope was done with MIPAR image analysis. The surface morphology analysis help to understand the deformation mechanism of the coatings during the incubation period. Through the use of thresholding in the software, the area ratios of the coating at different times under cavitation testing were found.

The images obtained from SEM shows that some sample had initial micro-cracks that occurred during the coating process. This phenomenon is visible on both the coating and substrate as can be seen in *Figure 11*. It is observed that for the CrN/TiN coated sample there are two distinct layers. This is due to the coating being removed and attached to the on top of the other surface.

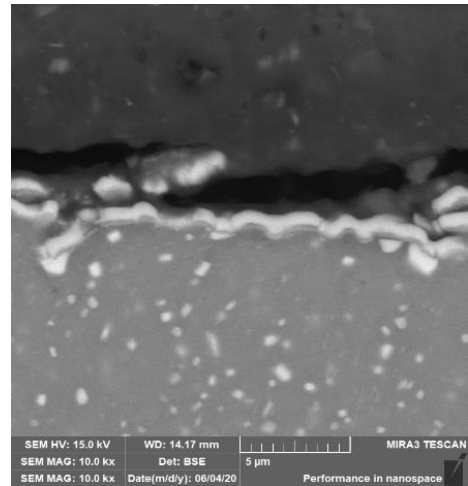
The hardness of the samples was examined by a Brinell - hardness tester. The sample's hardness was measured by a hydraulic pressed hardball at a load of 1N and a ball diameter of 1mm. The values obtained in BHN is presented below. The unit of BHN is kg force per sq. mm.

Table 3: BHN Hardness of samples

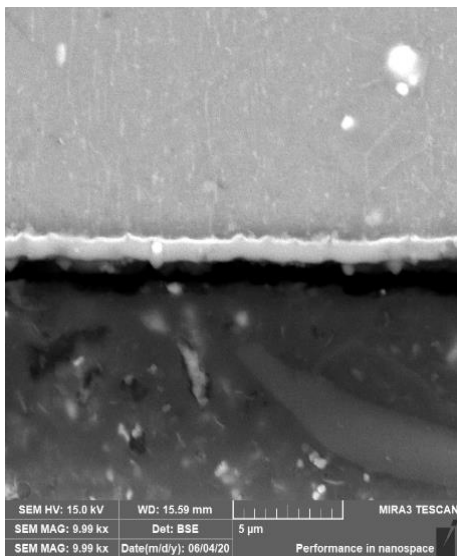
Sample	Hardness (BHN)
Raw	94.9
AlTiN	73.49
CrN/AlTiN	67.96
CrN	66.88
CrN/TiN	58.47
TiCN	58.24



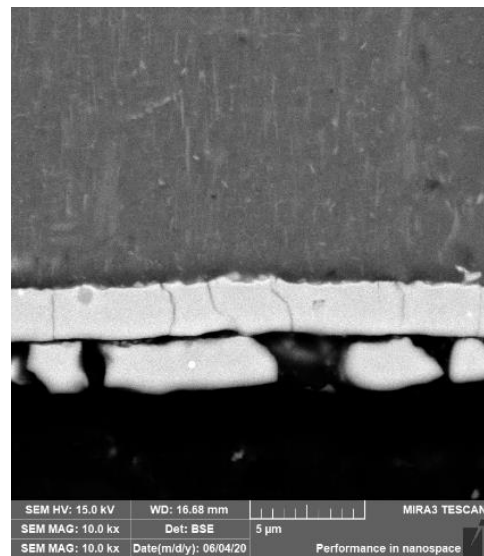
(a)



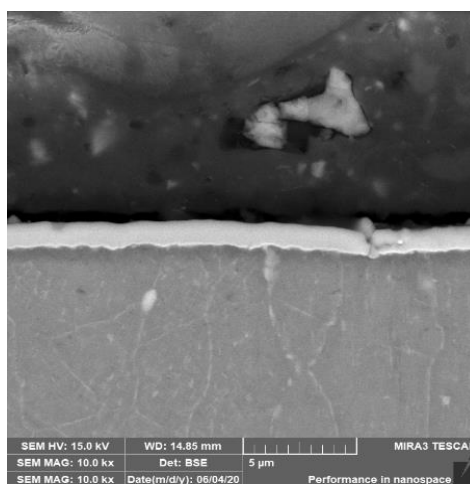
(b)



(c)



(d)



(e)

Figure 11: SEM microscope test of samples with (a)CrN coating (b)TiCN coating (c) AlTiN coating (d) CrN/TiN coating (e) CrN/AlTiN coating

## 4. Results

This chapter shows the results obtained from the sample's response to the cavitation test and the surface morphology throughout the process. The methods used in the analysis of the results are also described below.

### 4.1 Cavitation Erosion

Figure 12 shows the cumulative mass loss of the samples under the cavitation erosion test. While reading the cavitation curve of the raw duralumin, the incubation period and the erosion rate indicates that it has better resistance to cavitation than the coated samples and the reference sample. The incubation period was recorded to be 62 min and 30 sec. The coated samples all had a much shorter incubation period. The first mass loss for the single-layered sample of AlTiN and the multilayered samples of CrN/AlTiN and CrN/TiN coating was recorded after 20 min and 30 sec. The other samples had a relatively longer incubation period of 25:30 seconds and 40:30 seconds for the single-layered CrN and TiCN respectively.

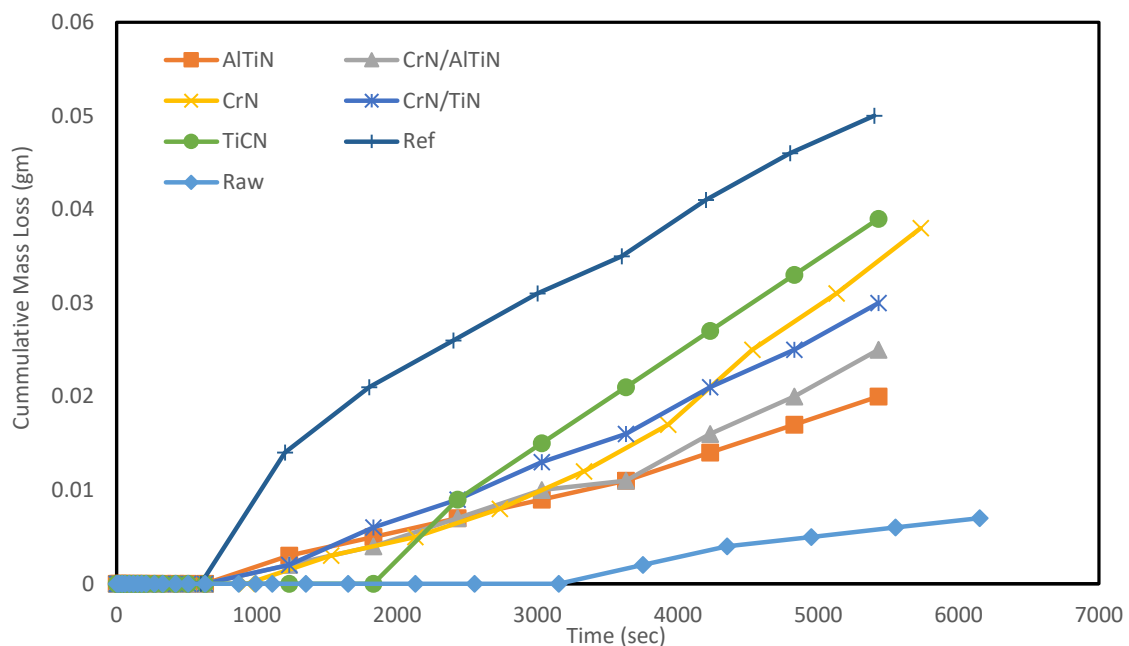


Figure 12: Cumulative mass loss under cavitation erosion test

This reduction in the incubation period for the coated samples is followed by the accelerated mass loss. Figure 13 shows the mass-loss rate of the samples under the cavitation test. The comparison of mass loss after 1 hour of testing showed that TiCN coated sample, which had the longest incubation period, had the highest mass loss of 0.021 gm. This is followed by CrN and CrN/TiN at 0.016 gm.

The samples with the shortest incubation period, AlTiN and CrN/AlTiN, had the least mass-loss of 0.011 gm. All the coated samples had less resistance to the cavitation erosion than the raw material, where the initial mass loss of 0.002 gm was recorded after 62:30 sec.

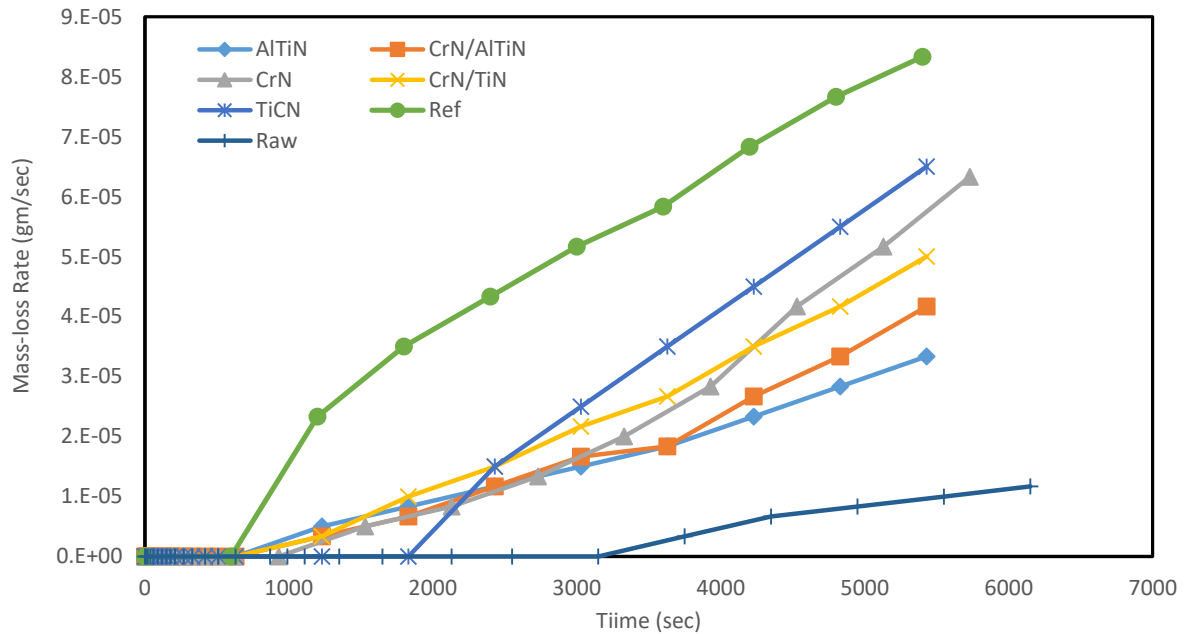


Figure 13: Erosion rate in cavitation erosion test

The reduction in the resistance to cavitation erosion is evident. In Figure 14, the cumulative mass-loss in time of the raw and reference sample is presented. This is to show that the coating process has affected the substrate of the samples. The incubation period was 20 min and the mass loss after an hour was recorded to be 0.035gm.

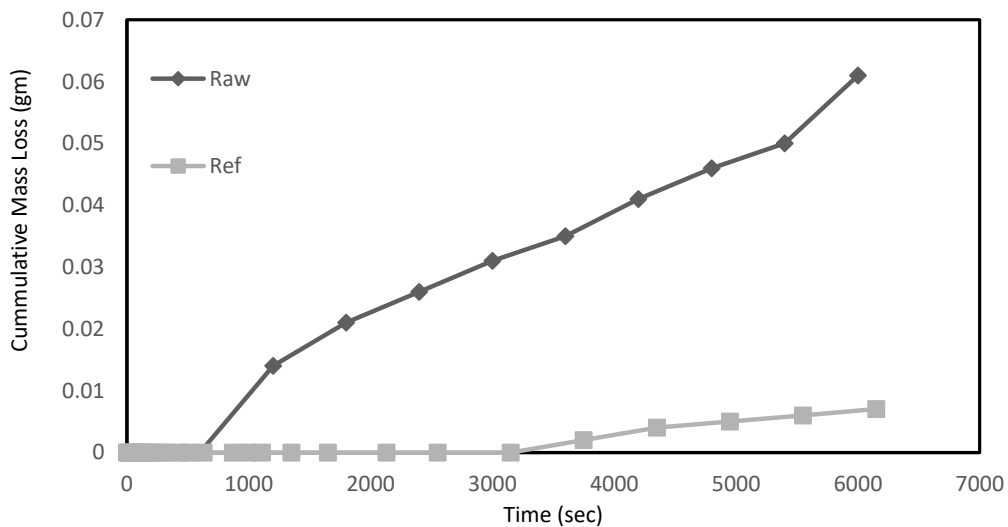
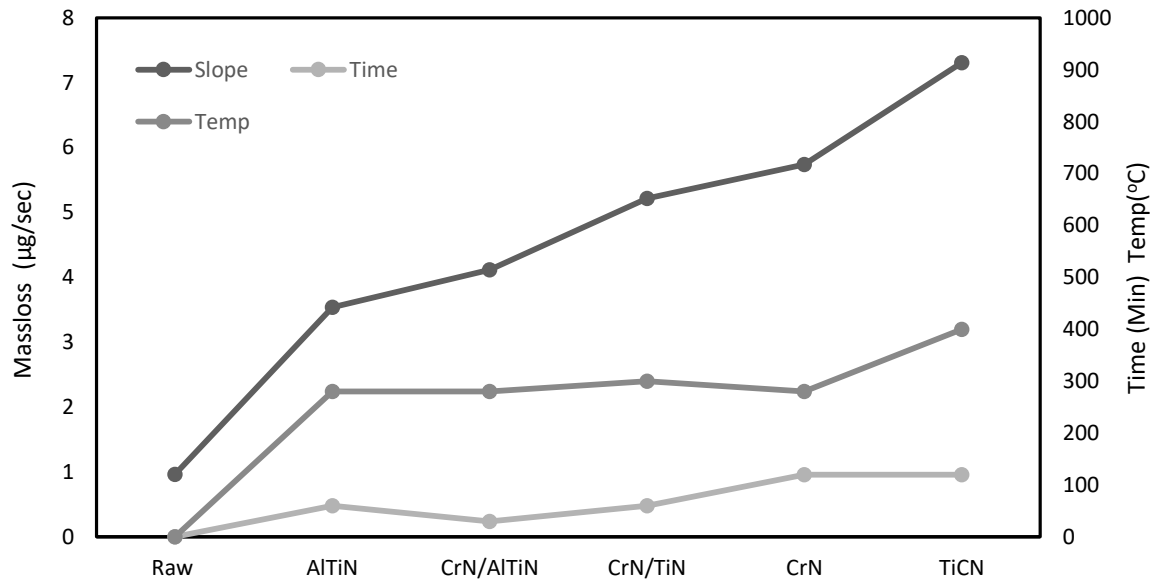


Figure 14 : Cumulative mass loss in time of raw and reference sample



The temperature and time of the coating process has influenced the resistance of the samples as can be seen in *Figure 15*. It is observed that the increase of temperature has increased the mass loss rate. This is because the substrate's, duralumin, mechanical properties such as hardness can be affected by exposure to high temperatures. Even though the exact relation is not found, the effect is still apparent.



*Figure 15: Effect of time and temperature of the coating process on the mass loss rate*

#### 4.2 Erosion mechanism

The surface morphology of the samples at different times is displayed in *Table 4*. The samples were scanned with the help of a confocal microscope. The area ratios of the samples were found using MIPAR Image analysis software. Small pores and scratches were noticed on the coating's surface before starting the experiment. The results also show that all the coatings were removed at the end of the incubation period as can be seen in *Table 4* and *Figure 16*. But the removal methods were different. Before the start of the cavitation test, CrN coated sample had scratches on the surface which further deepened during the cavitation test. At 10:30 sec time, it was seen that even though the cracks had formed the removal of the coating was small. Around 97.3 % was still covered by the coating. But due to the cracks further propagating the coating was completely removed and mass loss was recorded at 25:30 sec. AlTiN coated sample initially scratches or cracks on the surface were not observed but it was after a few minutes cracks started to form. These cracks propagated fast, where at 10:30 sec time period it is possible to see that the substrate is already being exposed. The area ratio of the coating was around 92.5%. After another 10 min it was seen that the coating has completely been removed and the substrate

was being eroded. The reason for this type of erosion mechanism is the difference in tensile stress between the substrate and the coating. Both the multi-layered samples also behaved similarly. After 10:30 sec of cavitation test, small cracks had formed where the substrates were exposed. The area ratio of the coatings was 98.4% and 95.1% for CrN/AlTiN and CrN/TiN coated samples respectively. This was followed by very fast removal of the coating. Sample with pits on the initial surface would increase in size as it is exposed to cavitation. This pattern was seen with the TiCN coated sample. The pits acted as a place of nucleation during the cavitation test. This leads to pits increasing in size as could be seen in *Table 4*, which through time kept on growing till neighboring pits intersected, and subsequently the coating material is completely eroded as can be seen in *Figure 16*.

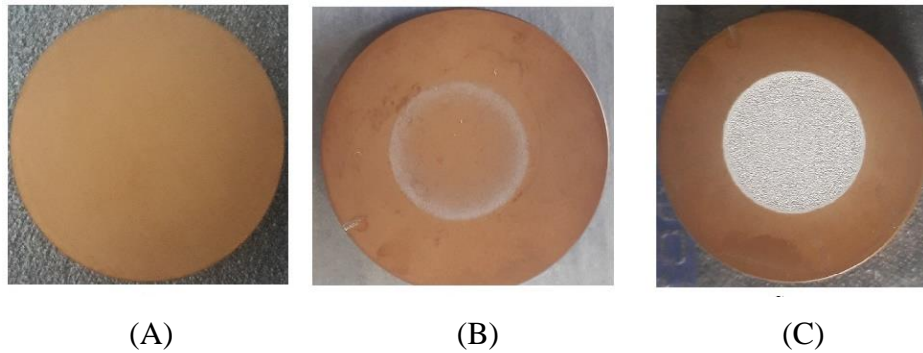


*Figure 16: TiCN coated sample (A) before cavitation test, (B) after 10:30 sec of exposure under cavitation and (C) after 40:30 sec exposure*

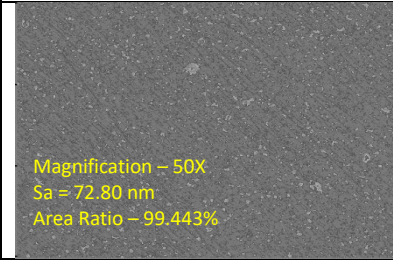
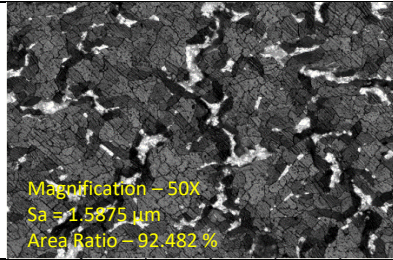
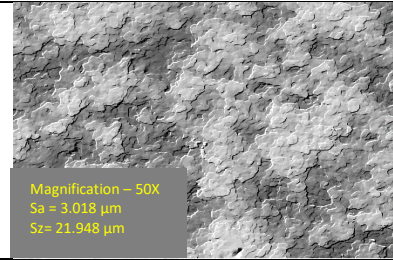
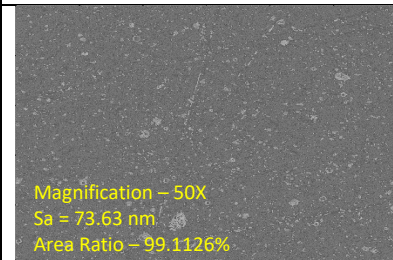
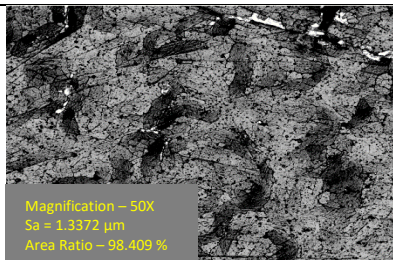
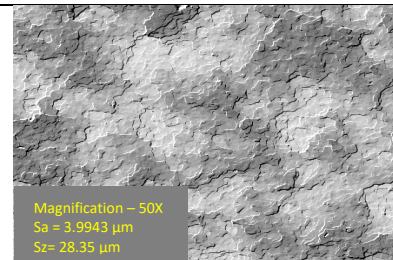
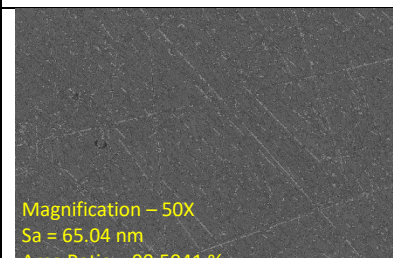
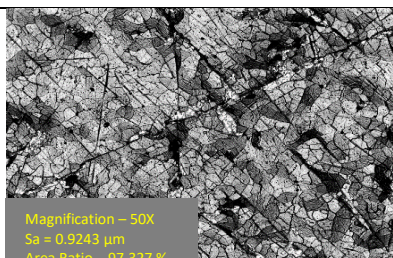
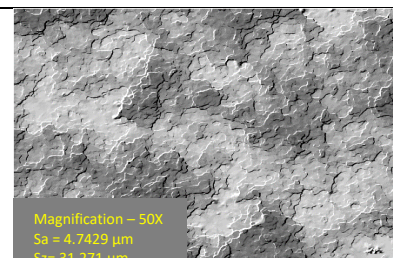
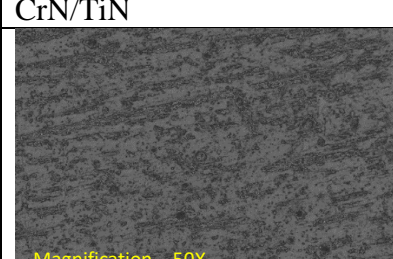
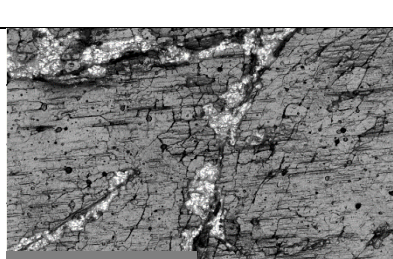
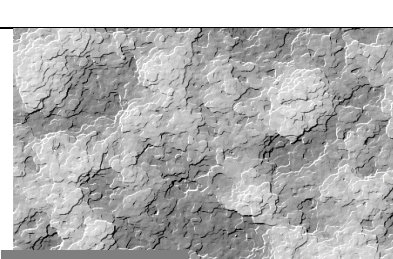
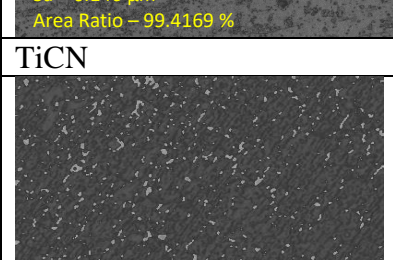
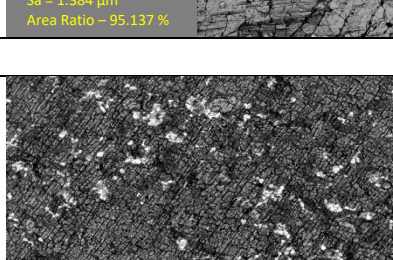
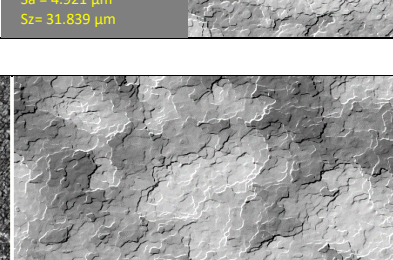
Initial state	10:30 sec after cavitation test	End of the incubation period
<b>AlTiN</b>		
 <p>Magnification – 50X Sa = 72.80 nm Area Ratio – 99.443%</p>	 <p>Magnification – 50X Sa = 1.5875 μm Area Ratio – 92.482 %</p>	 <p>Magnification – 50X Sa = 3.018 μm Sz= 21.948 μm</p>
<b>CrN/AlTiN</b>		
 <p>Magnification – 50X Sa = 73.63 nm Area Ratio – 99.1126%</p>	 <p>Magnification – 50X Sa = 1.3372 μm Area Ratio – 98.409 %</p>	 <p>Magnification – 50X Sa = 3.9943 μm Sz= 28.35 μm</p>
<b>CrN</b>		
 <p>Magnification – 50X Sa = 65.04 nm Area Ratio – 99.5941 %</p>	 <p>Magnification – 50X Sa = 0.9243 μm Area Ratio – 97.327 %</p>	 <p>Magnification – 50X Sa = 4.7429 μm Sz= 31.271 μm</p>
<b>CrN/TiN</b>		
 <p>Magnification – 50X Sa = 0.146 μm Area Ratio – 99.4169 %</p>	 <p>Magnification – 50X Sa = 1.384 μm Area Ratio – 95.137 %</p>	 <p>Magnification – 50X Sa = 4.921 μm Sz= 31.839 μm</p>
<b>TiCN</b>		
 <p>Magnification – 50X Sa = 0.1137 μm Area Ratio – 98.99 %</p>	 <p>Magnification – 50X Sa = 1.9287 μm Area Ratio – 94.563 %</p>	 <p>Magnification – 50X Sa = 9.127 μm Sz= 55.865 μm</p>

Table 4: Surface morphology of the samples at different time period



In Figure 17, the roughness parameter Sz (maximum height ) change during the incubation period is shown. The surface roughness parameter Sz does not indicate the duration of the incubation period. But rather the level of plastic deformation which takes place during the incubation period. The graph initially shows a near-linear relation between Sz and time. But as it progresses there is a change in slope, which is caused by an increase in plastic deformation and crack propagation. TiCN coated sample had the highest initial roughness which kept on increasing as time progressed. But TiCN coated sample was also recorded to have the longest incubation period. The rest of the samples' initial roughness correlates with the duration of the incubation period of the samples. The increase in the roughness of the samples is indicative of the formation and growth of pits. The raw sample had the smallest initial roughness and through time maintained a lower slope than the other samples. This shows that the roughness influences the resistance of the material to cavitation. But other parameters also have a large influence on erosion behavior. This can be seen on the TiN coated sample, which despite having a higher initial roughness and slope, had the longest incubation time.

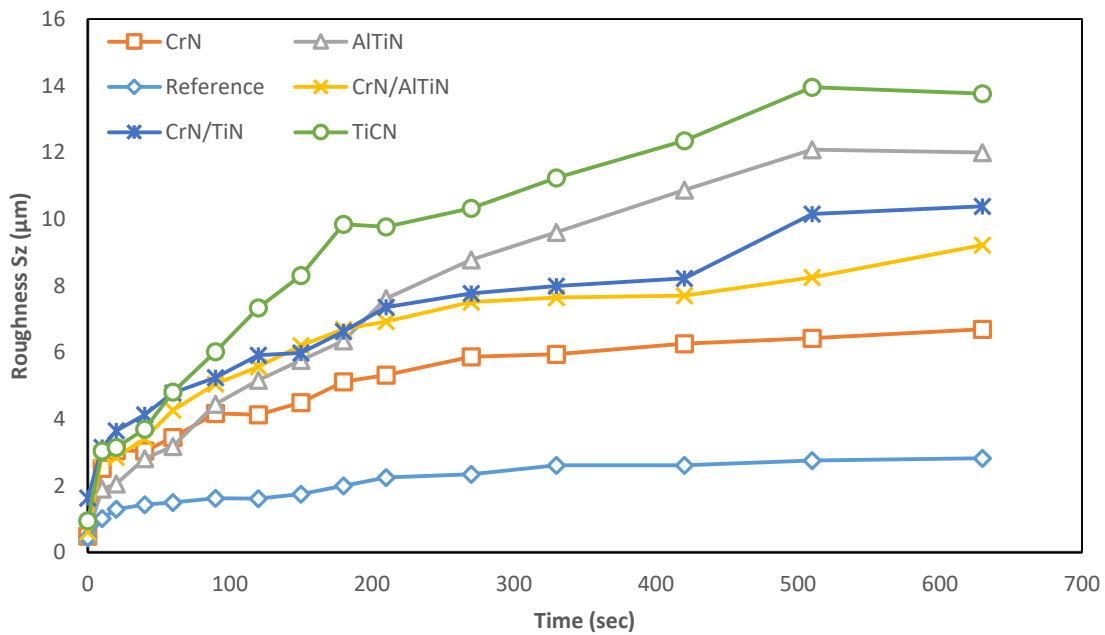
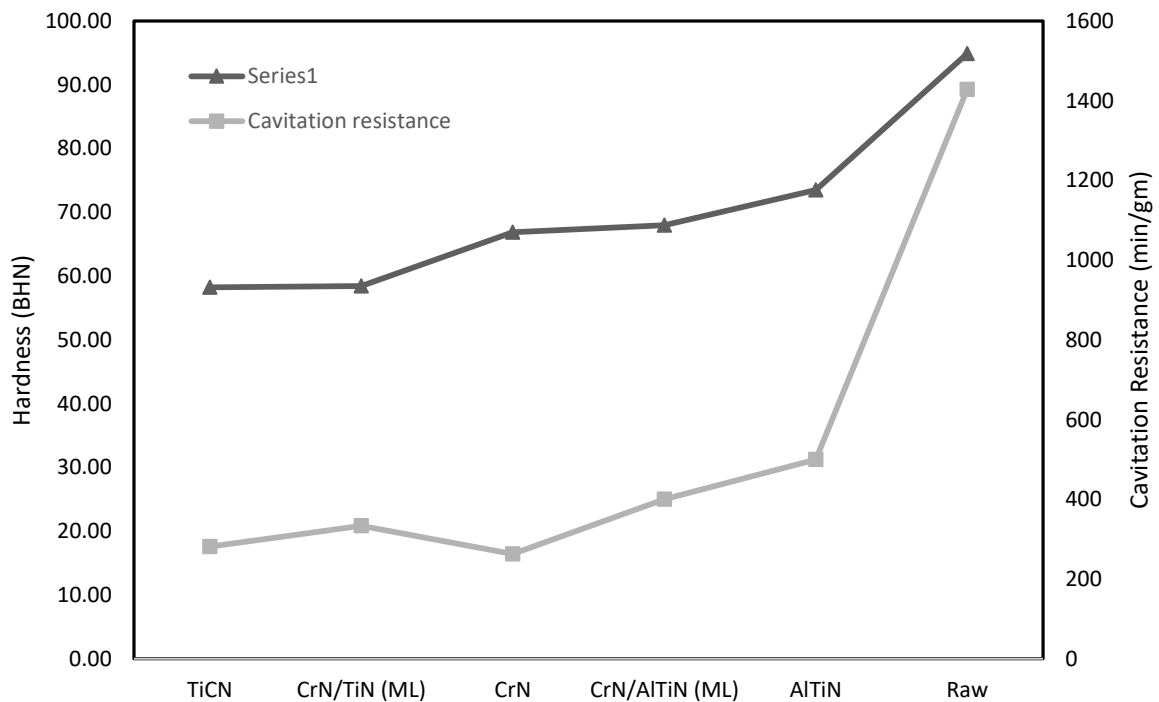


Figure 17: Change in Sz with time

### 4.3 Hardness

The hardness of the substrate was influenced by the coating process. This change in hardness of the substrate is one of the reasons for the reduction in resistance to cavitation erosion, as shown in *Figure 18*. The raw sample exhibits the highest hardness among the samples and is also the most resistant to cavitation erosion. But it is important to note that other factors also influence the resistance of the samples.



*Figure 18: Effect of hardness on samples' cavitation resistance*

## 5. Discussion

The results obtained show that the PVD coatings developed cavitation erosion wear with a roughened surface and plastically deformed, semi-brittle, eroded surface. The resistance to cavitation erosion has decreased. The cumulative mass loss and mass-loss rate of the coated samples were much higher than that of the raw sample, which can be observed in *Figure 12* and *Figure 13*.

To discuss the incubation period, the samples will be grouped into two. The first group are four of the samples coated with AlTiN, CrN, CrN/TiN, CrN/AlTiN, and the second group is TiCN coated sample. The classification is based on their incubation period, which by observing the graphs it is noticeable that the first group had a measurable mass loss at a similar time. When a sample has a higher incubation period it is due to better adhesion. The adhesion of the substrate can be influenced by different factors, one of which is the sample's pre-treatment (or sample preparation) before the coating process. The two groups had different sample pre-treatment methods. This could have influenced the sample's resistance to cavitation erosion as it can also be seen from the erosion mechanism.

During the examination of the failure mode, it was observed that the samples with scratches on the initial surface, had a failure mode similar to micro-ploughing mechanism. This was apparent in the AlTiN CrN/TiN and CrN/AlTiN coated samples. This resulted in early exposure of the substrate to the cavitation erosion. The cracks that propagated eventually aided the delamination of the coatings. CrN coated sample had a failure method similar to brittle fracture, where cracks were formed and propagating this led to the exposure of the substrate which eventually was completely removed. The progression from the substrate being exposed to complete delamination was fast. For TiCN coated sample, the initial surface has small pits that enlarged during the cavitation test. This reduced the removal rate of the coating resulting in a longer incubation period. SEM scan also showed that microcrack on both the surface and the coating were prevalent in the first group. The roughness was also affected by the pretreatment. In that, the second group's initial value and slope of the roughness throughout the entire process were higher. But the better adhesion was exhibited by the sample resulted in a higher incubation period.

The temperature and the time taken for coating the samples also influenced the adhesion of the coating to the substrate. The temperature is especially of interest because despite improving the adhesion it resulted in changing the mechanical properties of the substrate which influenced

the mass-loss rate. When discussing the mass loss, it should be noted that the recorded mass loss is from the loss of the substrate. As the coatings were very thin, recording its loss was not possible. The mass-loss rate of the samples, on the other hand, was influenced by the properties of the substrate, which was affected during the coating process, where the usage of high temperature influenced the loss of hardness of the substrate, duralumin. This can be seen in *Figure 19*. It can be observed that other parameters also have affected the hardness of the substrates.

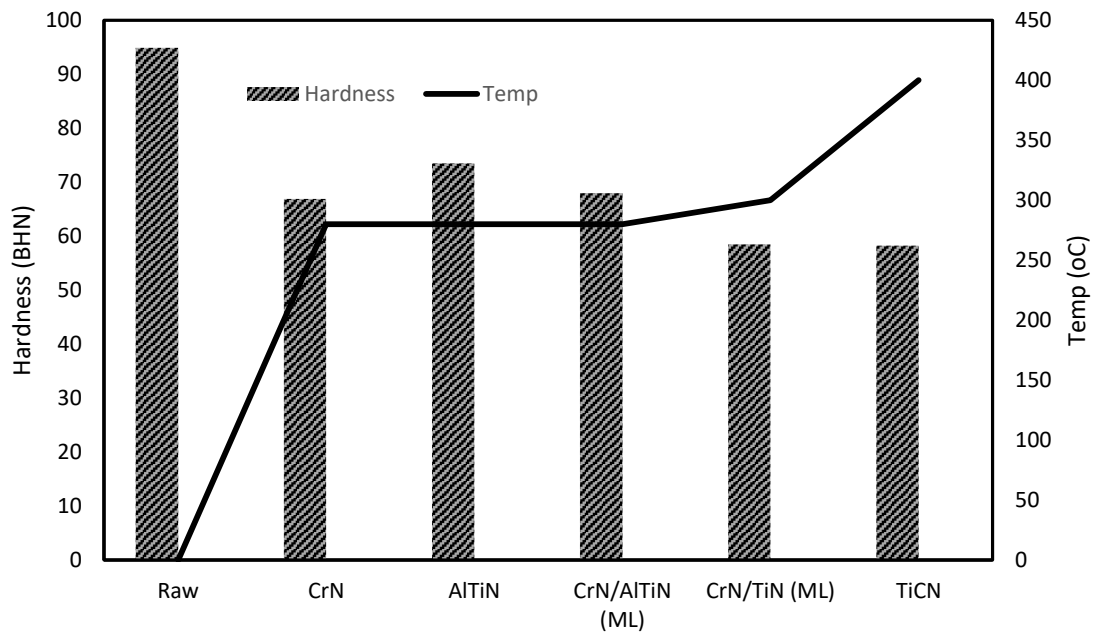


*Figure 19: Effect of temperature on hardness*

The hardness has influenced the mass-loss rate. TiCN coated sample which had one of the lowest measured hardness had the highest mass loss slope. The temperature used for coating was also the highest, 400°C. The cavitation resistance of the samples decreased with the decrease of the hardness. The CrN/TiN sample was coated at 300°C but had a similar hardness to TiCN, which is indicative that relating the hardness to the temperature or relating slope to the hardness, does not give a conclusive result. But it is still evident these parameters influence one another.

It is important to remember that in the ARC PVD coating process, the temperature is not an independent variable. But rather depends on the arc current, followed by the bias voltage and pressure of nitrogen in the vacuum chamber. To change the temperature changing these parameters would be necessary, which would result in changing the coating process. An

observation made was that the pressure of nitrogen in the vacuum chamber influenced the mass loss as presented *Figure 20*. The effect of the pressure of nitrogen in the vacuum chamber is not clear but the effect of the vacuum pressure is a point to consider in the future.

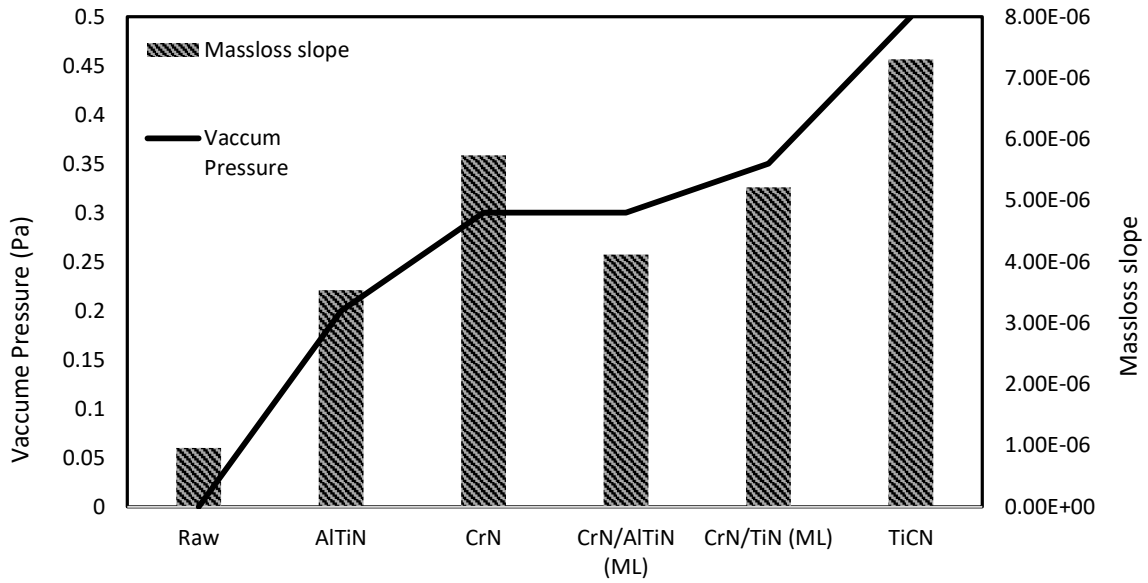


*Figure 20: The relation between Vacuum pressure and mass loss slope*



## 6. Conclusion

This thesis researched on improving cavitation erosion resistance by applying thin layers. The effect of the coating method on the material properties were highlighted. Multilayered samples and their single layered counterparts were examined. The experiment was carried out using vibratory cavitation apparatus, where the samples were exposed to the cavitation test for a short durations to find the incubation period. The samples were weighted and scanned using a confocal microscope, to measure the mass and roughness respectively.

The measurement of mass is to record initial mass loss which is indicative of the duration of the incubation period and the roughness helps characterize the coating's behavior under cavitation. SEM scan were obtained to characterize the substrates' interaction with the coating and to measure the thickness. The scan showed that the coating method has influenced the substrate. Further characterization was done by the use of Brinell - hardness tester. It was observed that the hardness was affected by the coating method. This resulted in decrease of the resistance of all the coated samples, as it was found to have shorter incubation period than the uncoated sample. For better analysis it is recommended to measure more mechanical properties such as porosity to understand the mass loss rate and adhesion of the coating to analyze the incubation period. The results obtained suggest that the improvement of the resistance to cavitation erosion by the application of Nano-layer, is heavily dependent on the coating method as it can influence the substrate's mechanical property. It is recommended that careful considerations should be taken in the selection of appropriate pretreatment of the substrate.

## Reference

- [1] LIN, Cui, Qing ZHAO, Xiaobin ZHAO a Ying YANG. Cavitation erosion of metallic materials. *International Journal of Georesources and Environment-IJGE (formerly Int'l J of Geohazards and Environment)*. 2018, **4**(1), 1–8.
- [2] TULLIS, J. Paul. *Hydraulics of pipelines: Pumps, valves, cavitation, transients*. B.m.: John Wiley & Sons, 1989.
- [3] VOGEL, A., W. LAUTERBORN a R. TIMM. Optical and acoustic investigations of the dynamics of laser-produced cavitation bubbles near a solid boundary. *Journal of Fluid Mechanics*. 1989, **206**, 299–338.
- [4] SHAH, Yatish T., A. B. PANDIT a V. S. MOHOLKAR. *Cavitation reaction engineering*. B.m.: Springer Science & Business Media, 2012.
- [5] OZONEK, Janusz. *Application of hydrodynamic cavitation in environmental engineering*. B.m.: CRC Press, 2012.
- [6] TAO, Yuequn, Jun CAI, Xiulan HUAI, Bin LIU a Zhixiong GUO. Application of hydrodynamic cavitation to wastewater treatment. *Chemical engineering & technology*. 2016, **39**(8), 1363–1376.
- [7] MANICKAM, Sivakumar a Muthupandian ASHOKKUMAR. *Cavitation: A Novel Energy-Efficient Technique for the Generation of Nanomaterials*. B.m.: CRC Press, 2014.
- [8] BRENNEN, Christopher E. *Cavitation and bubble dynamics*. B.m.: Cambridge University Press, 2014.
- [9] PLESSET, Milton S. a Andrea PROSPERETTI. Bubble dynamics and cavitation. *Annual review of fluid mechanics*. 1977, **9**(1), 145–185.
- [10] FRANC, Jean-Pierre, Michel RIONDET, Ayat KARIMI a Georges L. CHAHINE. Material and velocity effects on cavitation erosion pitting. *Wear*. 2012, **274**, 248–259.

- [11] KIM, Ki-Han, Georges CHAHINE, Jean-Pierre FRANC a Ayat KARIMI. *Advanced experimental and numerical techniques for cavitation erosion prediction*. B.m.: Springer, 2014.
- [12] ROY, Samir Chandra. *Modeling and analysis of material behavior during cavitation erosion*. B.m., 2015. PhD Thesis. b.n.
- [13] KRELLA, Alicja a Andrzej CZYŻNIEWSKI. Cavitation erosion resistance of Cr–N coating deposited on stainless steel. *Wear*. 2006, **260**(11–12), 1324–1332.
- [14] KRELLA, Alicja a Andrzej CZYZNIEWSKI. Influence of the substrate hardness on the cavitation erosion resistance of TiN coating. *Wear*. 2007, **263**(1–6), 395–401.
- [15] ZHU, Jianqiang. *Microstructure evolution of Ti-based and Cr cathodes during arc discharging and its impact on coating growth*. B.m., 2013. PhD Thesis. Linköping University Electronic Press.
- [16] MAKHLOUF, Abdel Salam Hamdy a Ion TIGINYANU. *Nanocoatings and ultra-thin films: technologies and applications*. B.m.: Elsevier, 2011.
- [17] KRELLA, Alicja K. The new parameter to assess cavitation erosion resistance of hard PVD coatings. *Engineering Failure Analysis*. 2011, **18**(3), 855–867.
- [18] AHMED, S. M., K. HOKKIRIGAWA a R. OBA. Fatigue failure of SUS 304 caused by vibratory cavitation erosion. *Wear*. 1994, **177**(2), 129–137.
- [19] HATTORI, Shuji a Takamoto ITOH. Cavitation erosion resistance of plastics. *Wear*. 2011, **271**(7–8), 1103–1108.
- [20] SANTA, J. F., J. A. BLANCO, J. E. GIRALDO a A. TORO. Cavitation erosion of martensitic and austenitic stainless steel welded coatings. *Wear*. 2011, **271**(9–10), 1445–1453.
- [21] KARIMI, A. Cavitation erosion of a duplex stainless steel. *Materials Science and Engineering*. 1987, **86**, 191–203.

- [22] PATELLA, Regiane Fortes, Thierry CHOFFAT, Jean-Luc REBOUD a Antoine ARCHER. Mass loss simulation in cavitation erosion: Fatigue criterion approach. *Wear*. 2013, **300**(1–2), 205–215.
- [23] HATTORI, Shuji, Ryohei ISHIKURA a Qingliang ZHANG. Construction of database on cavitation erosion and analyses of carbon steel data. *Wear*. 2004, **257**(9–10), 1022–1029.
- [24] HATTORI, Shuji a Eisaku NAKAO. Cavitation erosion mechanisms and quantitative evaluation based on erosion particles. *Wear*. 2001, **249**(10–11), 839–845.
- [25] KNAPP, R. T., J. W. DAILY a F. G. HAMMIT. Cavitation McGraw-Hill. *New York*. 1970, **2**.
- [26] HAMMITT, Frederick G. *Cavitation and multiphases flow phenomena*. B.m.: McGraw-Hill, 1980. BOOK.
- [27] HAMMITT, Frederick G. *Cavitation erosion state of art and predicting capability*. 1979.
- [28] LIANG, Liang, Youxia PANG, Yong TANG, Hao ZHANG, Hui LIU a Yu LIU. Combined wear of slurry erosion, cavitation erosion, and corrosion on the simulated ship surface. *Advances in Mechanical Engineering*. 2019, **11**(3), 1687814019834450.
- [29] KRELLA, Alicja K., Dominika E. ZAKRZEWSKA a Artur MARCHEWICZ. The resistance of S235JR steel to cavitation erosion. *Wear*. 2020, 203295.
- [30] NALWA, Hari Singh. *Handbook of nanostructured materials and nanotechnology, five-volume set*. B.m.: Academic Press, 1999.
- [31] TOMLINSON, W. J. a S. J. MATTHEWS. Cavitation erosion of aluminium alloys. *Journal of materials science*. 1994, **29**(4), 1101–1108.
- [32] DOJČINOVIĆ, Marina, Nada JOVIČIĆ a Ljiljana TRUMBULOVIĆ. CAVITATION RESISTANCE OF ALUMINUM ALLOY. nedatováno.

- [33] GOTTARDI, Gianmaria, Marialaura TOCCI, Lorenzo MONTESANO a Annalisa POLA. Cavitation erosion behaviour of an innovative aluminium alloy for Hybrid Aluminium Forging. *Wear*. 2018, **394**, 1–10.
- [34] VAIDYA, S. a C. M. PREECE. Cavitation erosion of age-hardenable aluminum alloys. *Metallurgical Transactions A*. 1978, **9**(3), 299–307.
- [35] CAMPBELL, John. *Castings*. B.m.: Elsevier, 2003.
- [36] GIRELLI, Luca, Marialaura TOCCI, Lorenzo MONTESANO, Marcello GELFI a Annalisa POLA. Investigation of cavitation erosion resistance of AlSi10Mg alloy for additive manufacturing. *Wear*. 2018, **402**, 124–136.
- [37] MÜNSTERER, S. a K. KOHLHOF. Cavitation protection by low temperature TiCN coatings. *Surface and Coatings technology*. 1995, **74**, 642–647.
- [38] MARYNIN, V. H. Erosion of vacuum-arc Ti–N coatings. *Materials Science*. 2003, **39**(3), 447–451.
- [39] KRELLA, Alicja a Andrzej CZYŻNIEWSKI. Investigation concerning the cavitation resistance of TiN coatings deposited on austenitic stainless steel at various temperatures. *Wear*. 2008, **265**(1–2), 72–80.
- [40] KRELLA, Alicja. Cavitation erosion of TiN and CrN coatings deposited on different substrates. *Wear*. 2013, **297**(1–2), 992–997.
- [41] CARTER, V. E. *Metallic Coatings for Corrosion Control: Corrosion Control Series*. B.m.: Newnes, 2013. 1.
- [42] DU, Jin, Jianfeng ZHANG a Chao ZHANG. Effect of Heat Treatment on the Cavitation Erosion Performance of WC–12Co Coatings. *Coatings*. 2019, **9**(10), 690.
- [43] CHI, SangKi, JinHwan PARK a MinYoung SHON. Study on cavitation erosion resistance and surface topologies of various coating materials used in shipbuilding industry. *Journal of Industrial and Engineering Chemistry*. 2015, **26**, 384–389.
- [44] KRELLA, Alicja. The influence of TiN coatings properties on cavitation erosion resistance. *Surface and Coatings Technology*. 2009, **204**(3), 263–270.

- [45] YOON, Soon Young, Seog-Young YOON, Won-Sub CHUNG a Kwang Ho KIM. Impact-wear behaviors of TiN and Ti–Al–N coatings on AISI D2 steel and WC–Co substrates. *Surface and Coatings Technology*. 2004, **177**, 645–650.
- [46] LIMA, M. M., C. GODOY, P. J. MODENESI, J. C. AVELAR-BATISTA, A. DAVISON a A. MATTHEWS. Coating fracture toughness determined by Vickers indentation: an important parameter in cavitation erosion resistance of WC–Co thermally sprayed coatings. *Surface and Coatings Technology*. 2004, **177**, 489–496.
- [47] KRELLA, A. Cavitation resistance of TiN nanocrystalline coatings with various thickness. *Advances in Materials Science*. 2009, **9**(2), 12–24.
- [48] THAKARE, M. R., J. A. WHARTON, R. J. K. WOOD a C. MENGER. Exposure effects of alkaline drilling fluid on the microscale abrasion–corrosion of WC-based hardmetals. *Wear*. 2007, **263**(1–6), 125–136.
- [49] SZALA, Mirosław a Mariusz WALCZAK. Cavitation erosion and sliding wear resistance of HVOF coatings. *Welding Technology Review*. 2018, **90**(10).
- [50] HOFFMANN, Michael R., Scot T. MARTIN, Wonyong CHOI a Detlef W. BAHNEMANN. Environmental applications of semiconductor photocatalysis. *Chemical reviews*. 1995, **95**(1), 69–96.
- [51] LI, Youji, Xiaodong LI, Junwen LI a Jing YIN. Photocatalytic degradation of methyl orange by TiO<sub>2</sub>-coated activated carbon and kinetic study. *Water research*. 2006, **40**(6), 1119–1126.
- [52] LINSEBIGLER, Amy L., Guangquan LU a John T. YATES JR. Photocatalysis on TiO<sub>2</sub> surfaces: principles, mechanisms, and selected results. *Chemical reviews*. 1995, **95**(3), 735–758.
- [53] HELLER, Adam. Chemistry and applications of photocatalytic oxidation of thin organic films. *Accounts of Chemical Research*. 1995, **28**(12), 503–508.
- [54] ALEXANDER, Bruce D., Pawel J. KULESZA, Iwona RUTKOWSKA, Renata SOLARSKA a Jan AUGUSTYNSKI. Metal oxide photoanodes for solar hydrogen production. *Journal of Materials Chemistry*. 2008, **18**(20), 2298–2303.

- [55] FARAJI, Ghader, Hyoung Seop KIM a Hessam Torabzadeh KASHI. *Severe plastic deformation: methods, processing and properties*. B.m.: Elsevier, 2018.
- [56] MATTOX, Donald M. *Handbook of physical vapor deposition (PVD) processing*. B.m.: William Andrew, 2010.
- [57] POLMEAR, Ian, David STJOHN, Jian-Feng NIE a Ma QIAN. *Light alloys: metallurgy of the light metals*. B.m.: Butterworth-Heinemann, 2017.
- [58] BROWN, Ian G. Cathodic arc deposition of films. *Annual review of materials science*. 1998, **28**(1), 243–269.
- [59] ANDERS, Simone, Sébastien RAOUX, Kannan KRISHNAN, Robert A. MACGILL a Ian G. BROWN. Plasma distribution of cathodic arc deposition systems. *Journal of applied physics*. 1996, **79**(9), 6785–6790.
- [60] ANDERS, S. a A. ANDERS. *XVIIth International Symposium on Discharges and Electrical Insulation in Vacuum, Berkeley, California*. B.m.: IEEE-INST ELECTRICAL ELECTRONICS ENGINEERS INC 345 E 47TH ST, NEW YORK, NY ..., 1996.
- [61] KELES, O., Y. TAPTIK, O. L. ERYILMAZ, M. URGEN a A. F. CAKIR. Optimization of ARC-PVD TiN coating process parameters by Taguchi technique. *Quality Engineering*. 1999, **12**(1), 29–36.
- [62] PANJAN, P., P. GSELMAN, D. KEK-MERL, M. ČEKADA, M. PANJAN, G. DRAŽIĆ, T. BONČINA a F. ZUPANIČ. Growth defect density in PVD hard coatings prepared by different deposition techniques. *Surface and Coatings Technology*. 2013, **237**, 349–356.
- [63] DULAR, Matevž, Bernd STOFFEL a Brane ŠIROK. Development of a cavitation erosion model. *Wear*. 2006, **261**(5–6), 642–655.
- [64] LI, Zifeng. Criteria for jet cavitation and cavitation jet drilling. *International Journal of Rock Mechanics and Mining Sciences*. 2014, **71**, 204–207.
- [65] KRELLA, A. K. a D. E. ZAKRZEWSKA. Cavitation erosion–phenomenon and test rigs. *Advances in Materials Science*. 2018, **18**(2), 15–26.

- [66] STELLER, Janusz a Bolesław Grzegorz GIREŃ. International Cavitation Erosion Test Final Report. 2015.
- [67] POLA, Annalisa, Lorenzo MONTESANO, Marialaura TOCCI a Giovina Marina LA VECCHIA. Influence of ultrasound treatment on cavitation erosion resistance of AlSi7 alloy. *Materials*. 2017, **10**(3), 256.
- [68] PETKOV, Nikolay, Totka BAKALOVA, Hristo BAHCHEDZHIEV, Petr LOUDA, Pavel KEJZLAR, Pavla CAPKOVA, Martin KORMUNDA a Petr RYSANEK. Cathodic Arc Deposition of TiCN Coatings-Influence of the C<sub>2</sub>H<sub>2</sub>/N<sub>2</sub> Ratio on the Structure and Coating Properties. In: *Journal of Nano Research*. B.m.: Trans Tech Publ, 2018, s. 78–91.
- [69] TOTKA, Bakalova, Petkov NIKOLAY, Bahchedzhiev HRISTO, Kejzlar PAVEL a Zdobinská PETRA. Tribological Properties of TiN/AlTiN and AlTiN/TiN nanomultilayer coatings. 2016.



## Appendix I

### Mass loss data

Table 5: Mass loss date for raw sample

Time	Mass (gm)	Cumulative mass loss (gm)	mass loss rate (gm/sec)
00 Sec	8.576	0	0
10 Sec	8.576	0	0
20 Sec	8.576	0	0
40 Sec	8.576	0	0
60 sec	8.576	0	0
90 sec	8.576	0	0
120 sec	8.576	0	0
150 sec	8.576	0	0
180 sec	8.576	0	0
210 sec	8.576	0	0
270 sec	8.576	0	0
330 sec	8.576	0	0
420 sec	8.576	0	0
510 sec	8.576	0	0
630 sec	8.576	0	0
14:30 sec	8.576	0	0
16:30 sec	8.576	0	0
18:30 sec	8.576	0	0
22:30 sec	8.576	0	0
27:30 sec	8.576	0	0
35:30 sec	8.576	0	0
42:30 sec	8.576	0	0
52:30 sec	8.576	0	0
62:30 sec	8.574	0.002	3.33E-06
72:30 sec	8.572	0.004	6.67E-06
82:30 sec	8.571	0.005	8.33E-06
92:30 sec	8.57	0.006	1.00E-05
102:30 sec	8.569	0.007	1.17E-05

## Mass Loss Data

Table 6: Mass loss data for AlTiN coated sample

Time	Mass (gm)	Cumulative mass loss (gm)	mass loss rate (gm/sec)
00 Sec	8.427	0	0
10 Sec	8.427	0	0
20 Sec	8.427	0	0
40 Sec	8.427	0	0
60 sec	8.427	0	0
90 sec	8.427	0	0
120 sec	8.427	0	0
150 sec	8.427	0	0
180 sec	8.427	0	0
210 sec	8.427	0	0
270 sec	8.427	0	0
330 sec	8.427	0	0
420 sec	8.427	0	0
510 sec	8.427	0	0
630 sec	8.427	0	0
20:30 sec	8.424	0.003	5E-06
30:30 sec	8.422	0.005	8.33E-06
40:30 sec	8.42	0.007	1.17E-05
50:30 sec	8.418	0.009	1.5E-05
60:30 sec	8.416	0.011	1.83E-05
70:30 sec	8.413	0.014	2.33E-05
80:30 sec	8.41	0.017	2.83E-05
90:30 sec	8.407	0.02	3.33E-05

## Mass Loss Data

Table 7: Mass loss data for AlTiN/CrN coated sample

Time	Mass (gm)	Cumulative mass loss (gm)	mass loss rate (gm/sec)
00 Sec	8.228	0	0
10 Sec	8.228	0	0
20 Sec	8.228	0	0
40 Sec	8.228	0	0
60 sec	8.228	0	0
90 sec	8.228	0	0
120 sec	8.228	0	0
150 sec	8.228	0	0
180 sec	8.228	0	0
210 sec	8.228	0	0
270 sec	8.228	0	0
330 sec	8.228	0	0
420 sec	8.228	0	0
510 sec	8.228	0	0
630 sec	8.228	0	0
20:30 sec	8.226	0.002	3.33E-06
30:30 sec	8.224	0.004	6.67E-06
40:30 sec	8.221	0.007	1.17E-05
50:30 sec	8.218	0.01	1.67E-05
60:30 sec	8.217	0.011	1.83E-05
70:30 sec	8.212	0.016	2.67E-05
80:30 sec	8.208	0.02	3.33E-05
90:30 sec	8.203	0.025	4.17E-05

## Mass Loss Data

Table 8: Mass loss data for CrN Coated Sample

Time	Mass (gm)	Cumulative mass loss (gm)	mass loss rate (gm/sec)
00 Sec	8.196	0	0
10 Sec	8.196	0	0
20 Sec	8.196	0	0
40 Sec	8.196	0	0
60 sec	8.196	0	0
90 sec	8.196	0	0
120 sec	8.196	0	0
150 sec	8.196	0	0
180 sec	8.196	0	0
210 sec	8.196	0	0
270 sec	8.196	0	0
330 sec	8.196	0	0
420 sec	8.196	0	0
510 sec	8.196	0	0
630 sec	8.196	0	0
15:30 sec	8.196	0	0
25:30 sec	8.193	0.003	5E-06
35:30 sec	8.191	0.005	8.33E-06
45:30 sec	8.188	0.008	1.33E-05
55:30 sec	8.184	0.012	2E-05
65:30 sec	8.179	0.017	2.83E-05
75:30 sec	8.171	0.025	4.17E-05
85:30 sec	8.165	0.031	5.17E-05
95:30 sec	8.158	0.038	6.33E-05

## Mass Loss Data

Table 9: Mass loss data for CrN/TiN coated sample

Time	Mass (gm)	Cumulative mass loss (gm)	mass loss rate (gm/sec)
00 Sec	8.395	0	0
10 Sec	8.395	0	0
20 Sec	8.395	0	0
40 Sec	8.395	0	0
60 sec	8.395	0	0
90 sec	8.395	0	0
120 sec	8.395	0	0
150 sec	8.395	0	0
180 sec	8.395	0	0
210 sec	8.395	0	0
270 sec	8.395	0	0
330 sec	8.395	0	0
420 sec	8.395	0	0
510 sec	8.395	0	0
630 sec	8.395	0	0
20:30 sec	8.393	0.002	3.33E-06
30:30 sec	8.389	0.006	1E-05
40:30 sec	8.386	0.009	1.5E-05
50:30 sec	8.382	0.013	2.17E-05
60:30 sec	8.379	0.016	2.67E-05
70:30 sec	8.374	0.021	3.5E-05
80:30 sec	8.37	0.025	4.17E-05
90:30 sec	8.365	0.03	5E-05

## Mass Loss Data

Table 10: Mass loss data for TICN coated sample

Time	Mass (gm)	Cumulative mass loss (gm)	mass loss rate (gm/sec)
00 Sec	8.197	0	0
10 Sec	8.197	0	0
20 Sec	8.197	0	0
40 Sec	8.197	0	0
60 sec	8.197	0	0
90 sec	8.197	0	0
120 sec	8.197	0	0
150 sec	8.197	0	0
180 sec	8.197	0	0
210 sec	8.197	0	0
270 sec	8.197	0	0
330 sec	8.197	0	0
420 sec	8.197	0	0
510 sec	8.197	0	0
630 sec	8.197	0	0
20:30 sec	8.197	0	0
30:30 sec	8.197	0	0
40:30 sec	8.188	0.009	1.5E-05
50:30 sec	8.182	0.015	2.5E-05
60:30 sec	8.176	0.021	3.5E-05
70:30 sec	8.17	0.027	4.5E-05
80:30 sec	8.164	0.033	5.5E-05
90:30 sec	8.158	0.039	6.5E-05